Title
Origin of ozone and NO_x in the tropical troposphere: A photochemical analysis of aircraft observations over the South Atlantic basin

Journal
Journal of Geophysical Research: Atmospheres, 101(D19)

ISSN
0148-0227

Authors
Jacob, DJ
Heikes, EG
Fan, S-M
et al.

Publication Date
1996-10-30

DOI
10.1029/96jd00336

JOURNAL OF GEOPHYSICAL RESEARCH, VOL. 101, NO. D19, PAGES 24,235–24,250, OCTOBER 30, 1996

Origin of ozone and NO_x in the tropical troposphere: A photochemical analysis of aircraft observations over the South Atlantic basin

D.J. Jacob,[1] B.G. Heikes,[2] S.-M. Fan,[1,3] J.A. Logan,[1] D.L. Mauzerall,[1] J.D. Bradshaw,[4] H.B. Singh,[5] G.L. Gregory,[6] R.W. Talbot,[7] D.R. Blake,[8] and G.W. Sachse,[6]

Abstract. The photochemistry of the troposphere over the South Atlantic basin is examined by modeling of aircraft observations up to 12-km altitude taken during the TRACE A expedition in September-October 1992. A close balance is found in the 0 to 12-km column between photochemical production and loss of O_3, with net production at high altitudes compensating for weak net loss at low altitudes. This balance implies that O_3 concentrations in the 0-12 km column can be explained solely by in situ photochemistry; influx from the stratosphere is negligible. Simulation of H_2O_2, CH_3OOH, and CH_2O concentrations measured aboard the aircraft lends confidence in the computations of O_3 production and loss rates, although there appears to be a major gap in current understanding of CH_2O chemistry in the marine boundary layer. The primary sources of NO_x over the South Atlantic Basin appear to be continental (biomass burning, lightning, soils). There is evidence that NO_x throughout the 0 to 12-km column is recycled from its oxidation products rather than directly transported from its primary sources. There is also evidence for rapid conversion of HNO_3 to NO_x in the upper troposphere by a mechanism not included in current models. A general representation of the O_3 budget in the tropical troposphere is proposed that couples the large-scale Walker circulation and in situ photochemistry. Deep convection in the rising branches of the Walker circulation injects NO_x from combustion, soils, and lightning to the upper troposphere, leading to O_3 production; eventually, the air subsides and net O_3 loss takes place in the lower troposphere, closing the O_3 cycle. This scheme implies a great sensitivity of the oxidizing power of the atmosphere to NO_x emissions in the tropics.

1. Introduction

Ozone in the tropical troposphere plays a key role in determining the global oxidizing power of the atmosphere. Most of the oxidation of long-lived gases by OH takes place in the tropics, where high UV and humidity promote the formation of OH from photolysis of O_3 [*Logan et al.*, 1981; *Thompson*, 1992]. Ozone is produced within the troposphere by photochemical oxidation of hydrocarbons and CO in the presence of nitrogen oxides (NO_x = NO + NO_2) and is also transported down from the stratosphere. There is continuing controversy as to the relative importance of tropospheric production versus stratospheric influx in controlling O_3 concentrations in the troposphere, including in the tropics [*Liu et al.*, 1980; *Levy et al.*, 1985; *Logan and Kirchhoff*, 1986; *Krishnamurti et al.*, 1993; *Dibb et al.*, 1996; *Graustein and Turekian*, 1996; *Browell et al.*, this issue; *Loring et al.*, this issue]. There is also considerable uncertainty regarding the origin of NO_x, the limiting precursor for O_3 production in the troposphere [*Levy and Moxim*, 1989; *Penner et al.*, 1991; *Kasibhatla et al.*, 1991, 1993].

We examine here the origin of O_3 and NO_x in the tropical troposphere using observations made during the TRACE A aircraft expedition in September-October 1992 [*Fishman et al.*, this issue]. This expedition provided a detailed survey of O_3 and its precursors over the tropical South Atlantic and neighboring continents up to 12-km altitude. Its primary objective was to identify the cause of the large-scale O_3 enhancement observed in the region during the austral spring dry season [*Fishman et al.*, 1990]. Results from TRACE A confirmed earlier suggestions that this enhancement is caused by seasonal biomass burning emissions of NO_x, hydrocarbons, and CO from southern Africa and South America [*Logan and Kirchhoff*, 1986; *Fishman et al.*, 1990; *Anderson et al.*, 1993; *Andreae et al.*, 1994; *Gregory et al.*, this issue; *Kirchhoff et al.*, this issue; *Olson et al.*, this issue; *Thompson et al.*, this issue].

Our goal in the present paper is to explain the total tropospheric O_3 column observed in TRACE A, not just the biomass burning enhancement, and to draw general inferences regarding the budget of O_3 in the tropical troposphere. As pointed out by

[1] Department of Earth and Planetary Sciences and Division of Applied Sciences, Harvard University, Cambridge, Massachusetts.
[2] Graduate School of Oceanography, University of Rhode Island, Narragansett, Rhode Island.
[3] Now at Department of Geology and Geophysical Sciences, Princeton University, Princeton, New Jersey.
[4] School of Earth and Atmospheric Sciences, Georgia Institute of Technology, Atlanta, Georgia.
[5] NASA Ames Research Center, Moffett Field, California.
[6] NASA Langley Research Center, Hampton, Virginia.
[7] Institute for the Study of Earth, Oceans, and Space, University of New Hampshire, Durham.
[8] Department of Chemistry, University of California at Irvine

Paper number 96JD00336.
0148-0227/96/96JD-00336$09.00

Thompson et al. [this issue], the tropospheric O_3 column over the South Atlantic during the dry season maximum is only 50% higher than the wet season background when biomass burning influence is minimal. This O_3 background, over the South Atlantic and elsewhere in the tropical troposphere, plays a critical role in determining the oxidizing power of the atmosphere.

Our analysis is based on a combination of photochemical modeling and statistical interpretation of the TRACE A data. The modeling approach is described in section 2 and is evaluated in sections 3 and 4 by simulation of H_2O_2, CH_3OOH, and CH_2O concentrations measured aboard the aircraft. Regional budgets for O_3 and NO_x over the South Atlantic basin are derived in sections 5 and 6, respectively. A general representation of the O_3 budget in the tropical troposphere is proposed in section 7. Conclusions are in section 8.

2. Modeling Approach

The TRACE A expedition used a DC-8 aircraft with a ceiling of 12-km altitude. The southern hemisphere flight tracks (Figure 1) covered the tropical South Atlantic, eastern Brazil, and southern Africa; we refer to this region as the "South Atlantic basin." Details on the flights and references for the observations are given by *Fishman et al.* [this issue]. Measurements aboard the aircraft included concentrations of O_3, CO, NO, peroxyacetylnitrate (PAN), peroxypropionylnitrate (PPN), HNO_3, speciated hydrocarbons, acetone, H_2O_2, CH_3OOH, CH_2O, and organic acids. Meteorological variables, UV fluxes, and aerosol number size distributions were also measured. Table 1 gives median values for the various measurements at different altitudes.

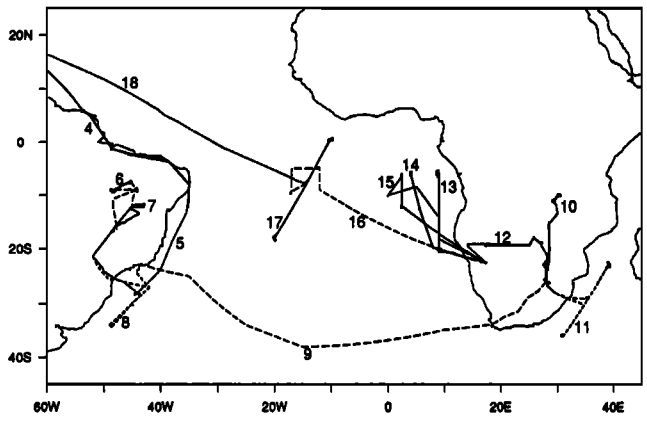

Figure 1. TRACE A flight tracks (September 23 - October 25, 1992). Flight numbers are indicated. The region covered by the southern hemisphere flight tracks is referred to in the paper as the South Atlantic basin.

We base our analyses on merged time series of the aircraft data where all measurements have been averaged over a common time interval. The choice of averaging interval must balance the need for high temporal resolution with the danger of misinterpret-

Table 1a. Median Measured Values Over the South Atlantic Basin During TRACE A

	Altitude		
	0-4 km	4-8 km	8-12 km
Temperature, K	284	258	230
Dew point, K	275	244	218
UV flux,[a] mW cm^{-2}			
zenith	4.7	5.3	5.8
nadir	0.75	1.5	2.0
O_3, ppbv	50	69	74
CO, ppbv	112	103	93
CH_4, ppbv	1695	1707	1715
NO, pptv	25	29	120
PAN, pptv	175	294	223
PPN, pptv	4	3	2
HNO_3, pptv	390	130	59
Ethane, pptv	590	630	670
Propane, pptv	48	46	58
$C_{4,5}$ alkanes, pptv	9	7	8
Ethene, pptv	21	8	9
Propene, pptv	6	4	4
Acetylene, pptv	130	130	110
Benzene, pptv	32	21	15
Toluene, pptv	7	2	<2
Acetone, pptv	750	593	650
Ethanol, pptv	60	<20	<20
HCOOH, pptv	1770	1000	560
CH_3COOH, pptv	3030	2550	1900
H_2O_2, pptv	2800	760	150
CH_3OOH, pptv	1200	320	60
CH_2O, pptv	200	<40	<40
Aerosol number, cm^{-3}			
0.12 to 0.2-μm radius	181	35	16
0.2 to 0.5-μm radius	310	28	8
0.5 to 2.0-μm radius	0.2	<0.1	0.3

Statistics are for the ensemble of southern hemisphere data collected in TRACE A. The median concentrations of $>C_5$ alkanes, $>C_3$ alkenes, xylenes, isoprene, and terpenes were below the detection limit of 2 pptv. Concentrations of NO_2 were measured in TRACE A, but the measurement is considered unreliable [*Crawford et al.*, 1996] and is not used in the paper.

[a] Measured with an Eppley radiometer (Eppley, Inc., Newport, Rhode Island)

Table 1b. Median Model Values Over the South Atlantic Basin During TRACE A

	Altitude		
	0-4 km	4-8 km	8.12 km
OH, 10^5 cm^{-3}	27	16	12
HO_2, 10^6 cm^{-3}	257	96	22
CH_3O_2, 10^6 cm^{-3}	103	34	3
NO_x=NO+NO_2, pptv	73	57	145
HNO_4, pptv	1	10	54

Twenty-four hour average model values computed as described in section 2. The concentration of NO_x is calculated in the model using as constraint the NO measurement for the time of day of observation

ing coarse-resolution data. We choose to average the data over the sampling time of the critical variable with the coarsest time resolution. Because this critical variable depends on the problem at hand, we will use over the course of this paper four different merged time series matched to the sampling times of peroxides, CH_2O, NO, and HNO_3 (Table 2). Ozone columns are included in the merged time series using daily observations with 1°x1.25° resolution from the total ozone mapping spectrometer (TOMS). The median O_3 column over the south tropical Atlantic during TRACE A was 281 Dobson units (DU) (1 DU = 2.687×10^{16} molecules cm^{-2}).

A major objective of this paper is to derive a chemical budget for O_3 in the tropospheric column over the South Atlantic basin (section 5). Our approach is to calculate 24-hour average O_3 production and loss rates for individual points in the merged time series of aircraft data and to use statistics from the ensemble of points to infer regionally averaged rates. Rapid chemical cycling takes place between O_3 and other members of the odd-oxygen family ($O_x = O_3 + O + NO_2 + HNO_4 + (2x)NO_3 + (3x)N_2O_5$ + peroxyacetylnitrates), hence the budget analysis must be based on O_x rather than on O_3. Considering that O_3 accounts typically for over 99% of O_x, the budgets of O_3 and O_x can be viewed as equivalent. Production of O_x is mainly by reactions (1) and (2):

$$HO_2 + NO \rightarrow OH + NO_2 \quad (1)$$

$$RO_2 + NO \rightarrow RO + NO_2 \quad (2)$$

where RO_2 is any organic peroxy radical (CH_3O_2 is the most important). Loss of O_x is principally by reactions (3)-(5):

$$O_3 + h\nu \rightarrow O_2 + O(^1D) \quad (3a)$$

$$O(^1D) + H_2O \rightarrow 2OH \quad (3b)$$

$$HO_2 + O_3 \rightarrow 2OH \quad (4)$$

$$OH + O_3 \rightarrow HO_2 + O_2 \quad (5)$$

Calculation of O_x production and loss rates requires knowledge of the concentrations of HO_x radicals (OH, HO_2, RO_2) along the flight tracks. These species were not measured from the aircraft. We estimate their concentrations for each point in the merged time series by using a zero-dimensional photochemical model constrained with the ensemble of measurements for that point (Table 3). The model is described in Appendix A. It calculates the diel steady state concentrations of HO_x radicals, short-lived NO_y species (NO, NO_2, NO_3, N_2O_5, HNO_2, HNO_4, organic nitrates), and other photochemical intermediates (peroxides, carbonyls). Production and loss of species are by chemical reactions only (loss by deposition is not considered). "Diel steady state" is defined by reproducibility of concentrations over a 24-hour solar cycle, as obtained in a time-dependent calculation with periodic boundary conditions

$$C_i(t) = C_i(t + T) \quad (6)$$

where C_i is the concentration of species i, t is time, and $T = 24$ hours. In this calculation, all input variables in Table 3 except NO are assumed constant over the diel cycle. The concentration of NO must be calculated as a time-dependent quantity because of the strong diel variation driven by photochemical steady state with NO_2. The few available observations in the remote troposphere indicate little diel variation of NO_x [*Carroll et al.*, 1992], but some variation might be expected in the upper troposphere due to cycling with HNO_4. We assume in the model that the concentration of NO_t ($NO + NO_2 + NO_3 + (2x)N_2O_5 + HNO_2 + HNO_4$) is constant over the diel cycle and calculate its value within the model to match the observed NO concentration at the time of day of the measurement.

Table 2. Merged Time Series of TRACE A Data

Matched Species	Time Resolution, min	Number of Points: Data	Number of Points: Model	Application
Peroxides	4-5	1254	223	a
CH_2O	1	1496	61 (926)	b
NO	3	1781	214 (1355)	c
HNO_3	2-15	721	201	d

Each data point represents one measurement time interval for the matched species. Model points are the subset of data points for which photochemical model quantities can be computed; the computation requires that data for all variables in Table 3 be available for at least a fraction of the time interval. We also give in parentheses the number of model points obtained in the fixed-hydrocarbon approximation, which relaxes the constraint on availability of data for hydrocarbons and acetone (see section 2).

[a] Comparison of simulated and observed peroxide concentrations (section 3).

[b] Comparison of simulated and observed CH_2O concentrations (section 4).

[c] O_3 production and loss rates and NO_2 concentrations (sections 5 and 6).

[d] Chemical budget of NO_x (section 6).

Table 3. Input Variables for the Photochemical Model Calculation

Variable Type	Variable
Meteorological	pressure, temperature, humidity
Radiation	solar declination, latitude, O_3 column,[a] cloud correction factor CF[b]
Chemical	O_3, CO, NO[c], PAN[d], HNO_3[d], methane[e], ethane, propane, C_{4-5} alkanes, C_{6-7} alkanes, ethene, propene, C_{4-6} alkenes, acetylene, benzene, toluene, xylenes, isoprene, acetone, ethanol, formic acid[e], acetic acid[e], aerosol number concentrations in three size classes[e,f]

[a] The total O_3 column is distributed vertically using the mean O_3 profiles measured by ozonesondes at Ascension Island and southern Africa during TRACE A [*Thompson et al.*, 1995].

[b] The cloud correction factor (CF) is calculated from the UV flux observations as described in Appendix A.

[c] The model calculation assumes a constant concentration of NO_t ($NO_t = NO + NO_2 + NO_3 + (2x)N_2O_5 + HNO_2 + HNO_4$) over the diel cycle and adjusts the concentration of NO_t to match the observed NO concentration at the time of day of observation.

[d] Data for HNO_3 and PAN are required only for the NO_x budget calculation of section 6. For other applications, if HNO_3 data are unavailable then a low value is assumed; and if PAN data are unavailable, then PAN concentrations are assumed from chemical steady state. These assumptions greatly increase the number of data points at which model calculations can be done without inducing significant error in the relevant model output quantities.

[e] If data are not available for these variables, default values are used of 1.7 ppmv for CH_4 and zero for formic acid, acetic acid, and aerosol number concentrations.

[f] See Table 1a for size class information.

Concentrations of H_2O_2, CH_3OOH, and CH_2O are calculated in the model, rather than constrained from observations, and comparison of simulated versus observed values serves to test the model (sections 3 and 4). These three species are sensitive to different aspects of HO_x chemistry [*Heikes*, 1992; *Liu et al.*, 1992]. Hydrogen peroxide is particularly valuable as a test of O_3 production in the model because its source,

$$HO_2 + HO_2 \rightarrow H_2O_2 + O_2 \quad (7)$$

varies quadratically with the concentration of HO_2, the principal peroxy radical responsible for O_3 production. At low altitudes where H_2O_2 is the principal sink of HO_x, the concentration of H_2O_2 reflects the rate of the $O(^1D)+H_2O$ reaction which is the principal source of HO_x and the principal sink of O_x.

We will also apply the model to study the chemical cycling of NO_x over the South Atlantic basin in light of the concurrent measurements of NO, HNO_3, and PAN made aboard the aircraft (section 6). Oxidation of NO_x to HNO_3 and PAN takes place on a timescale of the order of 1 day:

$$NO_2 + OH + M \rightarrow HNO_3 + M \quad (8)$$

$$NO_2 + O_3 \rightarrow NO_3 + O_2 \quad (9a)$$

$$NO_3 + NO_2 + M \rightarrow N_2O_5 + M \quad (9b)$$

$$N_2O_5 \xrightarrow{\text{aerosol},H_2O} 2HNO_3 \quad (9c)$$

$$NO_2 + CH_3CO_3 + M \rightarrow PAN + M \quad (10)$$

Organic nitrates other than PAN are also formed but represent only minor sinks for NO_x in the model. The species HNO_3 and PAN can act as reservoirs for NO_x, decomposing to release NO_x far from its point of origin:

$$HNO_3 + h\nu \rightarrow NO_2 + OH \quad (11)$$

$$HNO_3 + OH \rightarrow NO_3 + H_2O \quad (12a)$$

$$NO_3 + h\nu \rightarrow NO_2 + O \quad (12b)$$

$$PAN \xrightarrow{\text{heat}} NO_2 + CH_3CO_3 \quad (13)$$

$$PAN + h\nu \rightarrow NO_2 + CH_3CO_3 \quad (14)$$

We compute the 24-hour average rates of reactions (8)-(14) in the model at individual points using the observed concentrations of NO, HNO_3 and PAN as constraints, as discussed above. The resulting mass balance between sources and sinks of NO_x allows us to estimate the degree to which NO_x concentrations are maintained by chemical recycling from HNO_3 and PAN through the above set of reactions. In such a NO_x budget calculation it is necessary to correct the rates of conversion between NO_x and PAN to account for cycling within the (CH_3CO_3+PAN) family; the correction is described in Appendix B.

Table 1b gives the median concentrations of OH, HO_2, CH_3O_2, NO_x, and HNO_4 computed in the model for the southern hemisphere TRACE A data set. Diel steady state for these species and for CH_2O is typically approached to within 10% after 2 days of integration in the model. The peroxides, which have longer lifetimes, require typically 2-3 days at 2 km and 1 week at 8-12 km for approach to steady state. The steady state assumption is prone to large errors in pollution plumes and in the continental boundary layer, where concentrations of the input variables in Table 3 may change greatly over timescales of less than 1 day. It is more adequate in the free troposphere and in the marine boundary layer.

To conduct the model calculation for a given point in the merged time series we require that data be available for all variables in Table 3. Because of lack of temporal overlap in some of the measurements (notably NO, hydrocarbons, acetone), model calculations can be done for only a small fraction of the data points (Table 2). To increase the number of points, we use in certain applications a "fixed-hydrocarbon" version of the model in which we assume 630 parts per trillion by volume (pptv) C_2H_6 and 650 pptv acetone (mean values in TRACE A) and neglect the other nonmethane hydrocarbons. By relaxing the constraint on the availability of hydrocarbon and acetone data, the number of model points is greatly increased (Table 2). The errors incurred

by the fixed hydrocarbon approximation will be discussed in the context of each application. Data for HNO_3 and PAN are critical only for the NO_x mass balance analysis presented in section 6. For all other applications, when data for HNO_3 are missing a low value is assumed; and when data for PAN are missing the PAN concentration is assumed from chemical steady state. We verified that these assumptions have a negligible effect on HO_x levels and other relevant model results.

3. Peroxides

Figure 2 compares simulated and observed concentrations of H_2O_2 and CH_3OOH for individual points in the merged time series matched to the peroxide sampling times. Model values were sampled from the diel steady state cycle at the time of day of observation. Two outliers representing fresh fire plumes were excluded from the plots and from the statistics. Also shown on each plot are the least squares correlation coefficient r^2 between model and observations, the slope S of the linear best fit obtained by the reduced-major-axis method [*Hirsch and Gilroy*, 1984], and the median ratio R of simulated-to-observed concentrations. S and R offer different measures of model bias.

We find that the model captures 78% of the observed variance of H_2O_2 concentrations. This variance is determined strongly by water vapor (r^2 = 0.51 between observed H_2O_2 and H_2O mixing ratios). Median simulated-to-observed concentration ratios are 0.99 at 0-4 km, 0.87 at 4-8 km, and 0.57 at 8-12 km. Although H_2O_2 deposition is not included in the model, its effect should be largely limited to the mixed layer and to convective outflows because the lifetime of H_2O_2 against photochemical loss is relatively short (1.5 days below 2 km). The underestimate of H_2O_2 in the upper troposphere could reflect a missing HO_x source in the model but is also within the low-temperature uncertainties of the rate constants in the mechanism.

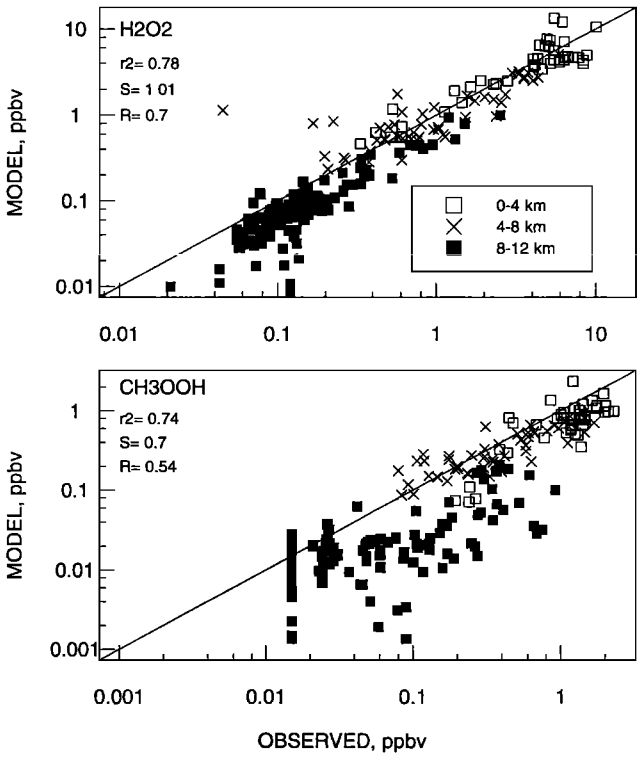

Figure 2. Simulated versus observed H_2O_2 and CH_3OOH concentrations in TRACE A. Also shown are the 1:1 line, the least squares correlation coefficient (r^2), the slope of the regression line (S), and the median ratio of simulated to observed concentrations (R). Observed CH_3OOH concentrations were below the detection limit of 15 pptv for 15% of the points.

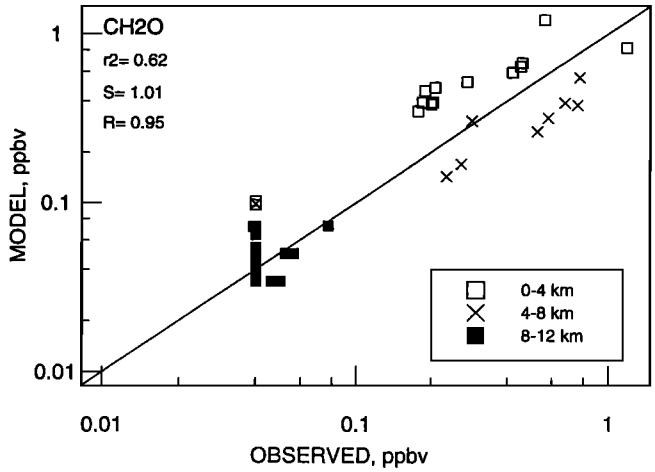

Figure 3. Simulated versus observed CH_2O concentrations in TRACE A. Also shown are the 1:1 line, the least squares correlation coefficient (r^2), the slope of the regression line (S), and the median ratio of simulated to observed concentrations (R). Observed concentrations were below the detection limit of 30-50 pptv for 56% of the points.

For CH_3OOH we find that the model captures 74% of the observed variance but is generally too low, particularly above 8 km. Median simulated-to-observed ratios are 0.59 at 0-4 km, 0.79 at 4-8 km, and 0.28 at 8-12 km. The underestimate is not outside the range of uncertainty of rate constants in the mechanism [*Thompson and Stewart*, 1991]. The estimated uncertainty on the rate constant for the reaction $CH_3O_2+HO_2$, which is the only CH_3OOH source in the model, is a factor of 2 at 298 K and a factor of 3 at 230 K [*DeMore et al.*, 1994]. Although the underestimate of CH_3OOH could suggest the presence of major hydrocarbon precursors missing from the model, we find no parallel underestimate of CH_2O that would support this hypothesis (see section 4).

The successful simulation of the peroxides below 8-km altitude lends confidence in the O_3 production and loss rates computed by the model. At 8 to 12-km altitude the ~ 40% underestimate of H_2O_2 could imply an ~ 20% underestimate of HO_2. Considering that HO_2 accounts for ~90% of total peroxy radicals in that altitude range (Table 1b), we may expect the O_3 production and loss rates above 8 km to be underestimated by about 20%.

Singh et al. [1995] pointed out the importance of acetone photolysis (included in our model) as a primary source of HO_x in the upper troposphere. We conducted a sensitivity calculation without acetone for the point representative of median conditions at 8-12 km (Table 1a). The H_2O_2, CH_3OOH, HO_2, and OH concentrations computed for that point decreased by 27% , 36%, 14%, and 16%, respectively, relative to the simulation including acetone. Neglecting acetone as a source of HO_x makes the model underestimate of peroxide concentrations in the upper troposphere significantly worse.

4. Formaldehyde

Figure 3 compares simulated and observed CH_2O concentrations for individual points in the merged time series matched to the CH_2O sampling times. Again, model values were sampled from the diel steady state cycle at the time of day of observation.

The model captures 62% of the observed variance. Model values tend to be too high in the lower troposphere (0-4 km) and too low in the middle troposphere (4-8 km). Most observations above 8 km are below the detection limit of 40 pptv.

Our ability to interpret model results for CH_2O is evidently hampered by the small number of model points. To address this problem, we turned to the fixed-hydrocarbon version of the model which provides 926 model points for comparison with observations. The fixed-hydrocarbon approximation gives only a lower limit for CH_2O, because it does not allow for the possibility of high hydrocarbon concentrations, but it still allows investigation of model overestimates. We find that the worst overestimate is in the marine boundary layer over the tropical South Atlantic (mean observed conditions 26 parts per billion by volume (ppbv) O_3, 66 ppbv CO, 3 pptv NO, 0.015 vol/vol H_2O), where the mean observed concentration of CH_2O is 0.11 ppbv (range <0.04-0.25 ppbv) while the corresponding model mean is 0.41 ppbv (range 0.28-0.55 ppbv). The mean observed H_2O_2 and CH_3OOH concentrations in that region are 2.3 ppbv and 1.1 ppbv, respectively, while the corresponding model means are 3.1 ppbv and 1.7 ppbv. The model shows some overestimate for the peroxides, which in the case of H_2O_2 could be due to deposition [*Heikes et al.*, this issue], but these discrepancies are small compared to CH_2O. We repeated the model calculation for the marine boundary layer points using observed concentrations of H_2O_2 and CH_3OOH as constraints, and assuming a deposition rate constant of 4×10^{-6} s^{-1} for CH_2O as representative of a deposition velocity of 0.4 cm s^{-1} over the ocean [*Thompson and Zafiriou*, 1983]. The mean CH_2O concentration in this calculation was 0.29 ppbv (range 0.21-0.48 ppbv), still 3 times higher than observed. The root of the discrepancy must therefore lie in the simulation of CH_2O chemistry.

Our model results for CH_2O can be viewed as typical of the current generation of photochemical models. We participated recently in an intercomparison of 20 models organized by the Intergovernmental Panel on Climate Change [*Prather et al.*, 1995]. In a test simulation representative of the remote marine boundary layer we obtained a CH_2O concentration of 0.21 ppbv, while other models obtained values ranging from 0.13 to 0.33 ppbv. The models at the low range had unusually high CH_2O photolysis frequencies.

We compared the marine boundary layer measurements of CH_2O in TRACE A to prior shipboard measurements made over the tropical Atlantic in the same season. *Lowe and Schmidt* [1983] measured a mean concentration of 0.20 ppbv (range 0.10-0.34 ppbv) at 30°N-30°S latitude with no significant latitudinal dependence. These values are higher than observed in TRACE A but still lower than in our model. *Harris et al.* [1992] used tunable diode laser spectroscopy to measure CH_2O concentrations in the northern tropics during the Polarstern cruise and found a mean concentration of 0.37 ppbv at 10°-20°N (they made no measurements farther south). During the same cruise, *Carlier et al.* [1991] reported mean CH_2O concentrations of 0.4 ppbv and 0.3 ppbv over the north and south tropical Atlantic, respectively. We evaluated our model against the *Harris et al.* [1992] data by taking as constraints the mean Polarstern observations at 15°N: 30 ppbv O_3, 90 ppbv CO, 1.3 ppbv H_2O_2, 15 pptv NO_2, 0.017 mol/mol H_2O, temperature of 293 K, and actinometer values of J_{NO_2} and J_{O^1D} [*Platt et al.*, 1992; *Jacob and Klockow*, 1992; *Brauers and Hofzumahaus*, 1992; *Hofzumahaus et al.*, 1992]. We obtained a model CH_2O concentration of 0.42 ppbv, in good agreement with the observations.

Other published measurements of CH_2O concentrations in clean tropical marine boundary layers include 0.4-1.1 ppbv over the Pacific [*Zafiriou et al.*, 1980; *Arlander et al.*, 1990] and 0.05-0.4 ppbv over the Indian Ocean [*Arlander et al.*, 1990]. It is not clear why there is such variability in the observations and why models are unable to reproduce the lower range of values. One possibility might be the complexation of CH_2O with organics in the marine aerosol. To our knowledge, the only concurrent gas phase and aerosol measurements of CH_2O in marine air are those of *Klippel and Warneck* [1980]. These authors found evidence that CH_2O in the aerosol is predominantly present as CH_2O complexes, but they also found that the aerosol contributes only a small fraction of total atmospheric CH_2O.

In summary, our results point to a major gap in current understanding of CH_2O concentrations in the marine boundary layer. Either some of the CH_2O measurements are flawed or a large CH_2O sink is missing from the models under some conditions. *Liu et al.* [1992] previously noted that CH_2O concentrations measured in free troposphere air at Mauna Loa, Hawaii (3.4-km altitude) were a factor of 3 lower than calculated from a standard photochemical model and attributed the discrepancy to a model overestimate of OH. However, later measurements by *Zhou et al.* [1996] at Mauna Loa indicated that the discrepancy is driven by a model overestimate of CH_3OOH and that CH_2O concentrations calculated in a model constrained with observed CH_3OOH are in good agreement with observations. A global three-dimensional photochemical model study by *Brasseur et al.* [1996] shows, in fact, good simulation of both CH_3OOH and CH_2O at Mauna Loa. We cannot draw a parallel between Mauna Loa and the marine boundary layer in TRACE A, because the discrepancy between model and observations for CH_2O in TRACE A is far greater than for CH_3OOH; also, as discussed above, there is no evidence in TRACE A for a model overestimate of CH_2O in the free troposphere. We searched the TRACE A data set for conditions that would approximate the Mauna Loa environment described by *Liu et al.* [1992] and *Zhou et al.* [1996], but all TRACE A measurements at that altitude had much lower temperatures and humidities than at Mauna Loa (temperature and humidity are important variables controlling CH_2O concentrations in the model).

5. Ozone

Plates 1a and 1b show the horizontal distributions of the 24-hour average gross production rate of odd oxygen, P_{O_x}, and the net production rate, $(P-L)_{O_x}$, at different altitudes in TRACE A. The rates were computed for the merged time series matched to the NO sampling time, using the fixed-hydrocarbon approximation in order to maximize the number of model points. The errors on P_{O_x} and L_{O_x} caused by the fixed-hydrocarbon approximation are small; for those points where the full model (including hydrocarbons) can be applied, the median ratio of P_{O_x} calculated in the full versus fixed-hydrocarbon versions of the model is $1.02\pm0.09(1\sigma)$ when P_{O_x} is less than 20 ppbv day^{-1}. This regime represents 92% of all observations in TRACE A and all observations outside the continental boundary layer. Plate 1b indicates a broad region of net photochemical loss exceeding 4 ppbv day^{-1} at 1.5 to 4-km altitude off the southwestern coast of Africa. This rapid loss is made possible by the albedo of persistent marine stratus decks. Gross photochemical production in the region is also high.

We see from Plate 1 that the gross production of O_3 decreases on average with altitude while the net production increases with altitude. Median vertical profiles of P_{O_x} and L_{O_x} for the southern hemisphere TRACE A data are plotted in Figure 4, and a summary O_3 budget for the 0 to 12-km column is given in Table 4. Both production and loss decrease with altitude, due to decreasing humidity, but production decreases slower than loss above 6 km because of high concentrations of NO. Above 6 km, photochemistry switches from a net sink to a net source of O_3. Similar transitions have been reported in previous model studies of the remote troposphere [*Liu et al.*, 1980; *Thompson and Cicerone*, 1982; *Davis et al.*, 1996]. Figure 4 indicates net production of O_3 taking place below 2-km altitude, but this portion of the budget is highly uncertain because of the large variability of O_3 production rates for individual points; there is a sharp contrast between the

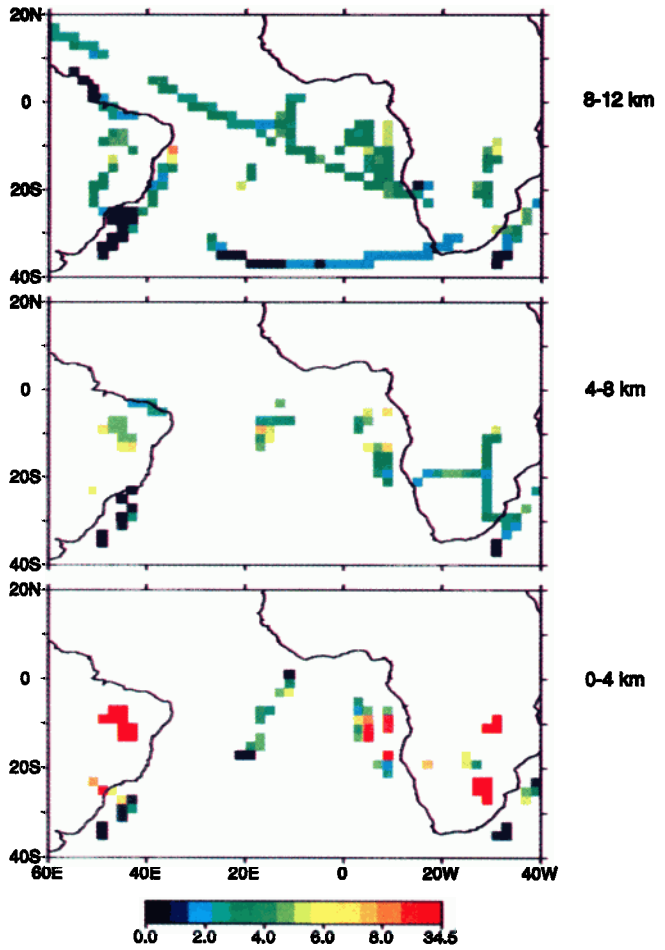

Plate 1a. Twenty-four-hour average gross production rates of odd oxygen (O_x = O_3 + O + NO_2 + HNO_4 + (2x)NO_3 + (3x)N_2O_5 + peroxyacetylnitrates) computed at 0 to 4-km, 4 to 8-km, and 8 to 12-km altitude in TRACE A.

continental boundary layer, where biomass burning influence can result in rapid O_3 production, and the marine boundary layer, where NO_x levels are low and O_3 production is slow (Plate 1). The point modeling approach is also most prone to errors in the continental boundary layer, as discussed in section 2.

We take the values in Figure 4 as our best estimates of the regionally averaged rates of O_3 production and loss over the South Atlantic basin. The corresponding integrals of P_{O_x} and L_{O_x} for the 0 to 12-km column are both 1.1×10^{12} cm^{-2} s^{-1}. These values are two orders of magnitude larger than the mean stratospheric influx of O_3 in the southern hemisphere troposphere estimated to be $1\text{-}3 \times 10^{10}$ cm^{-2} s^{-1} [*Gidel and Shapiro*, 1980; *Levy et al.*, 1985]. Even allowing for a slightly higher cross-tropopause flux in spring [*Holton*, 1990] and for preferential subsidence of air over the south tropical Atlantic [*Krishnamurti et al.*, 1993; *Loring et al.*, this issue], it is clear that stratospheric influx is a negligible contributor to tropospheric O_3 in the region. In situ photochemistry dominates even in the upper troposphere; the 4-km integral of P_{O_x} at 8 to 12-km altitude is 1.1×10^{11} cm^{-2} s^{-1}.

Deposition has only a small effect on the O_3 budget in the 0 to 12-km column. *Heikes et al.* [this issue] estimated a deposition flux to the Atlantic Ocean of 1.7×10^{10} cm^{-2} s^{-1} during TRACE A. *Fan et al.* [1990] measured a 24-hour average O_3 deposition flux of 10×10^{10} cm^{-2} s^{-1} to the Amazon forest in the wet season; scaling this flux to the ratio of dry and wet season O_3 concentrations over the forest [*Browell et al.*, 1990] would imply a dry season deposition flux to the Amazon forest of 17×10^{10} cm^{-2} s^{-1}. Another term in the O_3 budget is the time tendency, but this term is also small. Seasonal trends in the tropospheric O_3 column at sites in the South Atlantic basin are of the order of 5 DU per month, or 5×10^{10} molecules cm^{-2} s^{-1} [*Olson et al.*, this issue].

The close balance between chemical production and chemical loss of O_3 in the 0 to 12-km column implies that the total column amount of O_3 can be explained by in situ photochemistry, with net production above 6-km altitude balancing weak net loss below. To demonstrate this point, we conducted a one-dimensional photochemical steady state model calculation for O_3 in the 0 to 12-km column, fixing as input the median vertical profiles of O_3 precursors and other conditions from Table 1a and adopting a zero-flux upper boundary condition at 12-km altitude. The calculation assumed an O_3 deposition velocity of 0.05 cm s^{-1}, a uniform vertical eddy diffusion coefficient $K_z = 3 \times 10^5$ cm^2 s^{-1}, and 24-hour average clear-sky photolysis rates. Results in Figure 5 show that it is possible to explain the O_3 concentrations and vertical gradients observed in the 0 to 12-km column in TRACE A without invoking any exogenous O_3 source.

The median lifetime of O_x against chemical loss over the South Atlantic basin is 6 days at 0-4 km, 25 days at 4-8 km, and

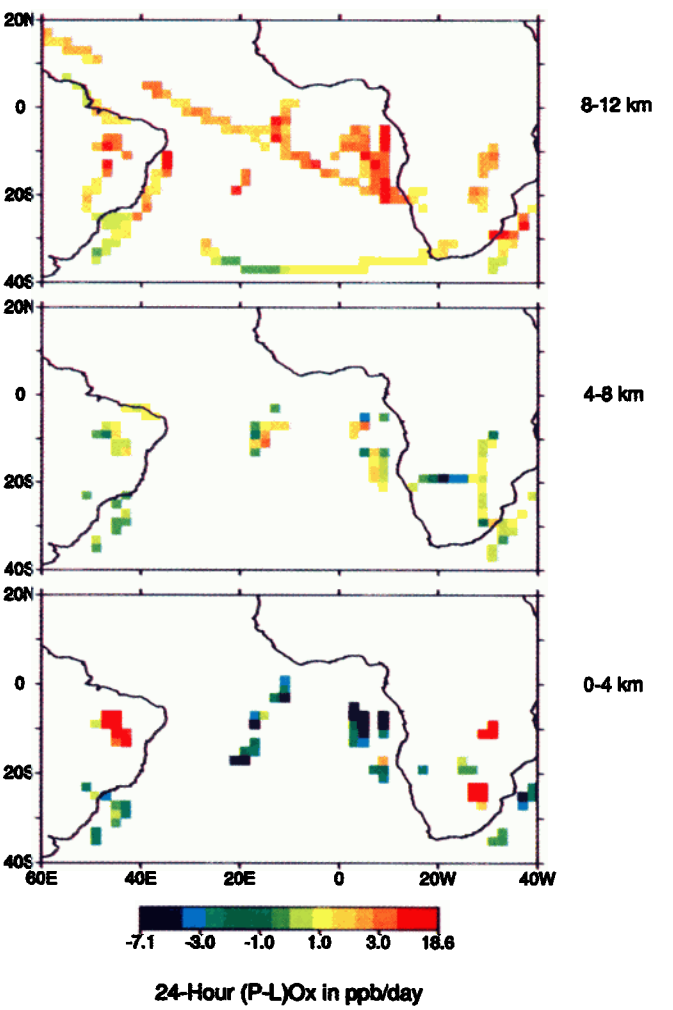

Plate 1b. Twenty-four-hour average net O_x production rates computed at 0 to 4-km, 4 to 8-km, and 8 to 12-km altitude in TRACE A.

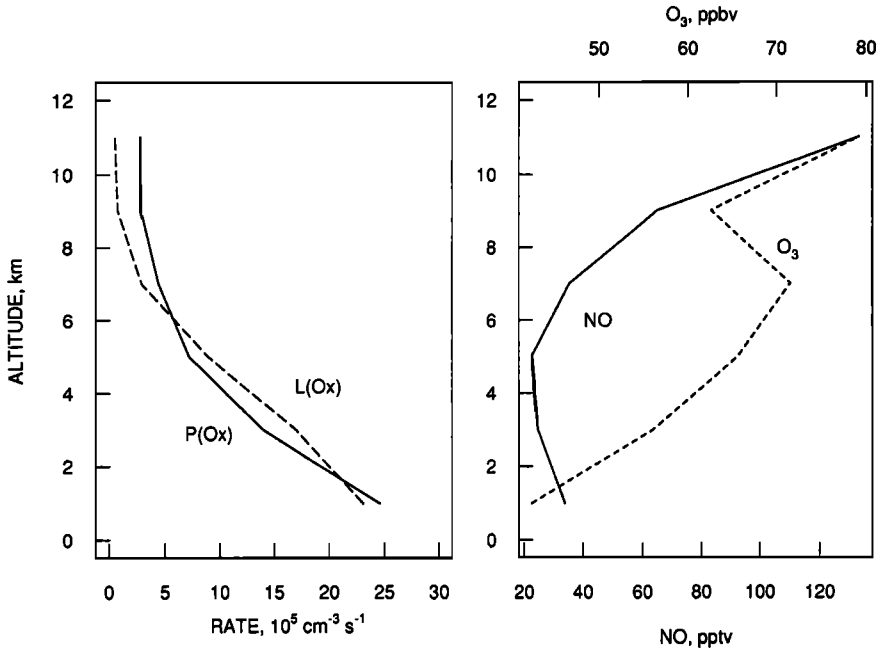

Figure 4. (Left) Median 24-hour average production and loss rates of O_x in the southern hemisphere TRACE A data as a function of altitude. (Right) Median concentrations of O_3 and NO.

105 days at 8-12 km (Table 4). As the altitude increases, the loss of O_3 becomes increasingly controlled by subsidence. Subsidence from the upper to the lower troposphere over the South Atlantic takes place on a timescale of the order of 10 days [*Krishnamurti et al.*, this issue]; we thus expect a characteristic time of about 2 weeks for O_3 to adjust to chemical steady state in the 0 to 12-km column. Such a characteristic time is sufficiently long that horizontal mass exchange with other regions could represent an important term in the budget of tropospheric O_3 over the South Atlantic basin. However, it appears from our close regional balance between chemical production and loss that this term does not provide either a major net source or a major net sink of O_3 in the South Atlantic basin troposphere, i.e., that the horizontal flux divergence is small. A general representation of the O_3 budget in the tropical troposphere consistent with this view is presented in section 7.

Tropospheric O_3 columns observed over the South Atlantic basin during the wet season are about 40% lower than observed in TRACE A [*Kirchhoff et al.*, 1991; *Olson et al.*, this issue; *Thompson et al.*, this issue]. We examined whether these wet season columns could be sustained by in situ photochemical production in the same way as in TRACE A. For this purpose we decreased the NO and CO levels in the one-dimensional model to represent an atmosphere unaffected by biomass burning. *Singh et al.* [1990] reported a median NO concentration of 8 pptv at 0 to 6-km altitude over the Amazon basin in April-May (wet season), with little vertical gradient. *Drummond et al.* [1988] reported a median NO concentration of 60 pptv at 11.5-km altitude between Rio de Janeiro and Dakar in June, at the beginning of the dry season when biomass burning influence is small and tropospheric O_3 columns still assume wet season values [*Kirchhoff et al.*, 1991]. We took these observations, which are about 3 times lower than in TRACE A, as constraints in the model. We further adopted a background CO concentration of 50 ppbv. Hydrocarbon concentrations were not modified from their values in Table 1a because they have little effect on O_3 production. As shown in Figure 5,

Table 4. Budget of Tropospheric Ozone Over the South Atlantic Basin

	Altitude, km		
	0-4	4-8	8-12
	Number of Model Points		
	292	246	574
Production and loss, ppbv d^{-1}			
P_{Ox}	8.0	3.8	2 9
L_{Ox}	9.0	3.6	0 7
$(P-L)_{Ox}$	-0.7	0 3	2 1
Column rates, 10^{10} cm^2 s^{-1}			
P_{Ox}	77	23	11
L_{Ox}	80	24	3
$(P-L)_{Ox}$	-6	2	8
O_3 lifetime ($[O_3]/L_{Ox}$), days	6	25	105
O_3 replacement time ($[O_3]/P_{Ox}$), days	7	20	24

Median 24-hour average rates and characteristic times computed in the model for the southern hemisphere TRACE A data. O_x is odd oxygen ($O_x = O_3 + O + NO_2 + HNO_4 + (2x)NO_3 + (3x)N_2O_5$ + peroxyacylnitrates). Column rates refer to the 4-km altitude bands. Because values are medians instead of means, $(P-L)_{Ox}$ and P_{Ox} - L_{Ox} are not identical.

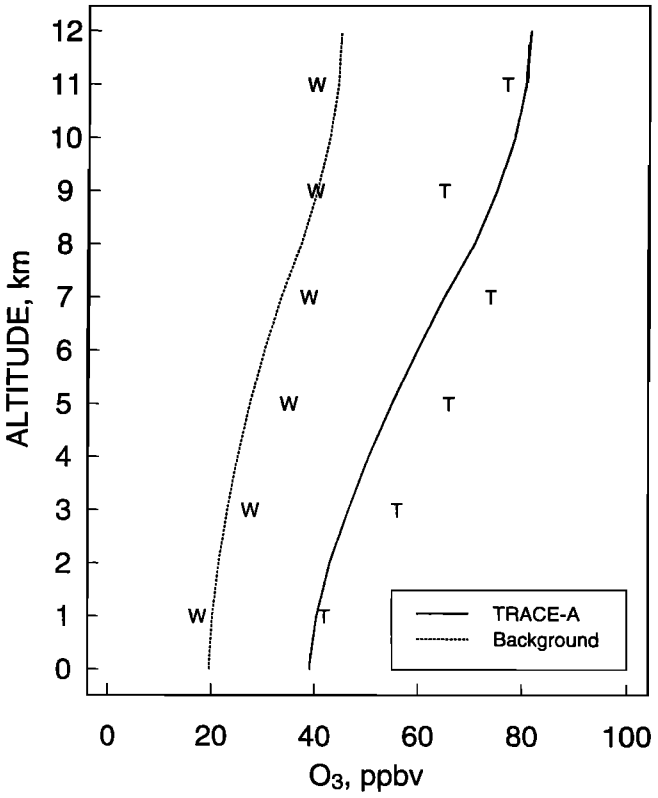

Figure 5. Steady state O_3 concentrations computed in a one-dimensional photochemical model constrained with the median TRACE A observations for O_3 precursors (solid line) and with NO and CO concentrations reduced to reflect a background atmosphere free of biomass burning influence (dotted line). The model uses a zero-flux boundary condition at 12-km altitude. The "T" symbols are the median O_3 concentrations in the southern hemisphere TRACE A data. The "W" symbols are the mean wet season (March-May) O_3 concentrations observed at Natal, Brazil [*Kirchhoff et al.*, 1991].

the vertical O_3 profile computed in the one-dimensional model is consistent with the mean wet season ozonesonde observations by *Kirchhoff et al.* [1991] at Natal, Brazil. It thus appears that the tropospheric O_3 column over the South Atlantic basin during the wet season can be sustained fully by in situ production, similarly to the dry season. Although NO_x levels are lower than in the dry season, the O_3 levels to be sustained are also lower.

The above analysis implies a strong sensitivity of tropospheric O_3 over the South Atlantic basin to the supply of NO_x. We show in Figure 6 the dependence of the net O_3 production rate on NO_x concentrations in the model for points representing the median conditions observed in TRACE A at 0 to 4 km, 4 to 8 km, and 8 to 12-km altitude (Table 1a). Even at the relatively high NO_x concentrations observed in TRACE A, O_3 production is still NO_x limited throughout the 0 to 12 km column. A number of authors have noted that NO_x levels in the remote troposphere are near the turnover point for net O_3 production versus net loss [*Chameides et al.*, 1987, 1990; *Jacob et al.*, 1992; *Liu et al.*, 1992; *Mauzerall et al.*, 1996; *Carroll and Thompson*, 1995], and this is also found in the TRACE A data below 8 km (Figure 6). Based on the discussion above, we explain this general result as reflecting the tendency of O_3 to approach a chemical steady state determined by the NO_x concentration.

6. Nitrogen Oxides

Several authors have examined the primary sources of NO_x over the South Atlantic basin in TRACE A by correlating the observed NO concentrations with chemical variables and with back-trajectories [*Smyth et al.*, this issue; *Singh et al.*, this issue; *Talbot et al.*, this issue; *Pickering et al.*, this issue]. They conclude that biomass burning was a major source of NO_x throughout the tropospheric column, and that lightning was also a major and perhaps dominant source in the upper troposphere. Soil emissions would provide an additional source of NO_x in the continental boundary layer [*Jacob and Wofsy*, 1988, 1990] but the TRACE A data are not well suited for assessing the importance of this source. Transport from the stratosphere was a negligible contributor to the NO_x budget even in the upper troposphere [*Smyth et al.*, this issue].

Chemical cycling between NO_x and its oxidation products played probably a major role in maintaining high NO_x concentrations over the South Atlantic during TRACE-A. The mean lifetime of NO_x against reactions (8)-(10) computed in the model for the TRACE A conditions is only 4 hours at 0-4 km and 2.4 days at 8-12 km. Plate 2 shows the distribution of NO_x concentrations over the South Atlantic basin as a function of longitude and altitude (NO is measured and NO_2 is from the photochemical model). Concentrations are high in the continental boundary layer and the upper troposphere, consistent with primary sources

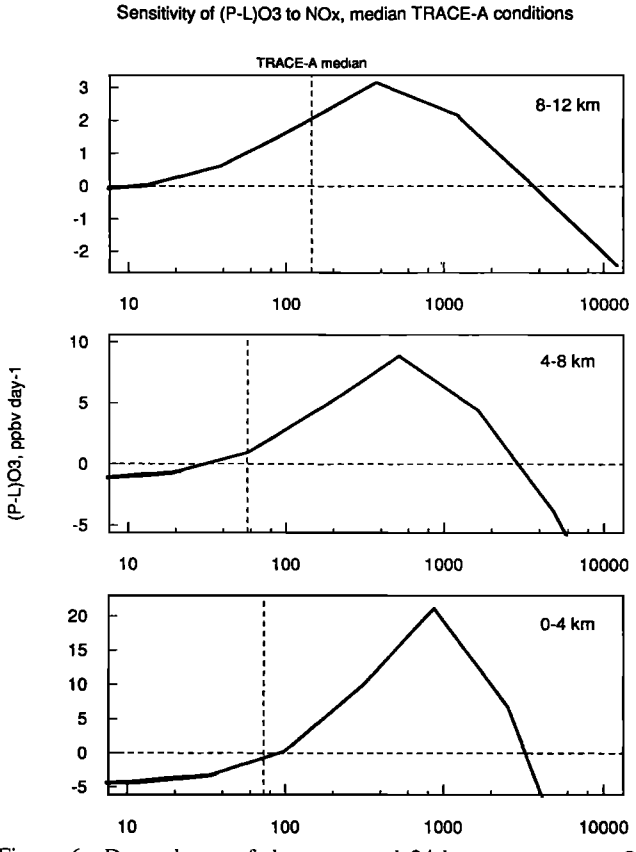

Figure 6. Dependence of the computed 24-hour average net O_3 production rate on NO_x concentrations for the TRACE A conditions. All variables other than NO_x are specified at their median TRACE A values given in Table 1a for 0-4, 4-8, and 8-12 km altitude. The dashed vertical lines show the median NO_x concentrations in the southern hemisphere TRACE A data for the different altitude bands.

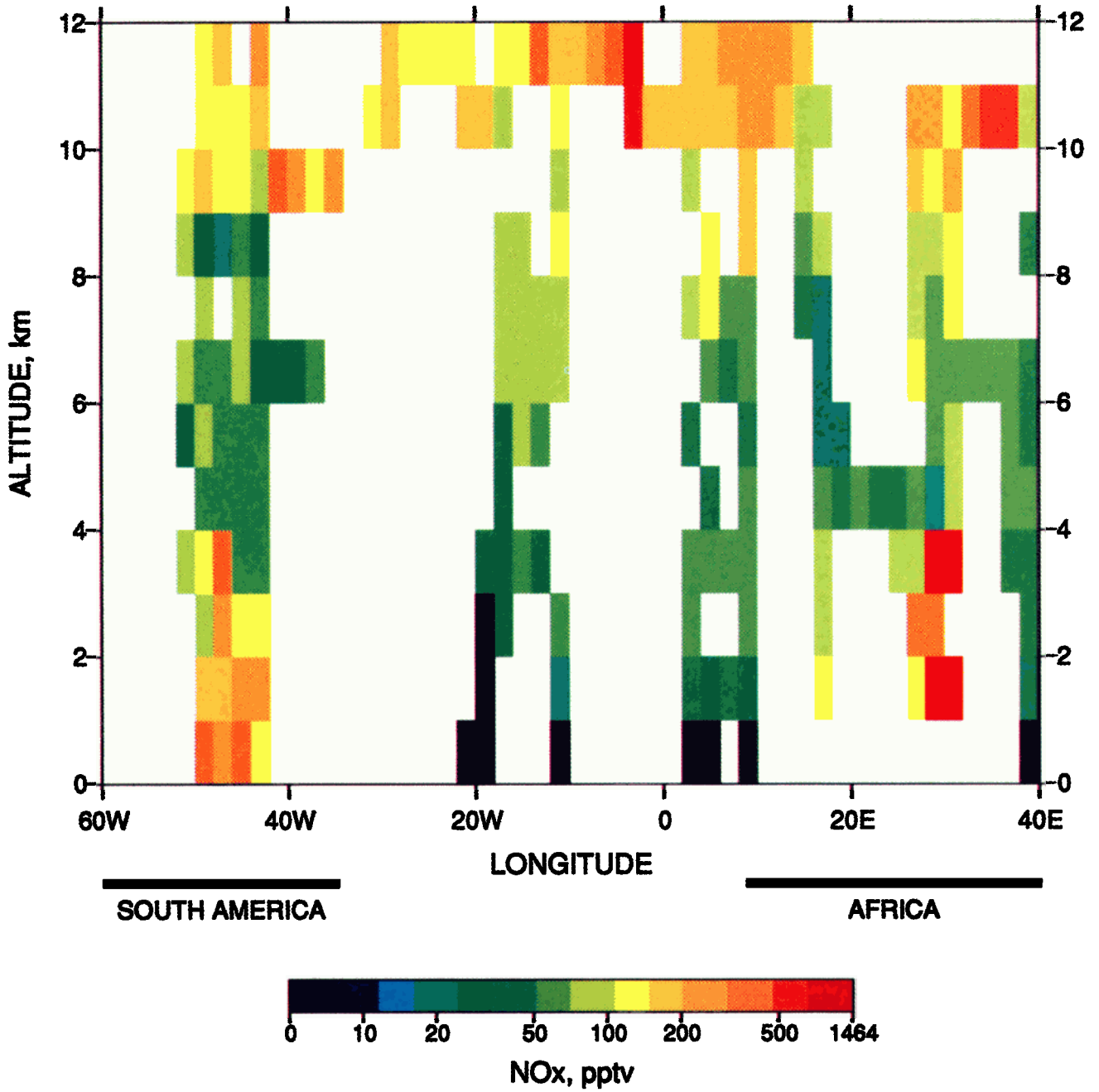

Plate 2. Mean concentration of NO_x in TRACE A at 0°-30°S latitude, as a function of longitude and altitude.

from combustion, soils, and lightning; during deep convective events over the continents, NO_x from combustion and soils is injected to the upper troposphere, and additional NO_x is produced by lightning. However, above 4 km we find no significant decrease of NO_x from continents to oceans, even though the primary sources of NO_x are continental (there is little lightning over the oceans) and the lifetime of NO_x is short. It appears that the high concentrations over the oceans must be maintained by chemical recycling.

We used our photochemical model to diagnose the degree to which NO_x levels in TRACE A could be maintained by chemical recycling based on current understanding of tropospheric chemistry. For this purpose we computed the chemical production and loss rates of NO_x at individual points in the merged time series matched to the HNO_3 sampling times, using the model constrained with measurements of NO, HNO_3, and PAN (details of the approach are given in section 2). Figure 7 shows the ratio of chemical loss to chemical production of NO_x for individual points as a function of altitude, and Table 5 summarizes the contributions of individual reactions to the NO_x budget at different altitudes. Below 4 km there is considerable scatter for individual points, reflecting primarily the relative abundances of NO_x and PAN; on average, we find a balance between the source of NO_x from decomposition of PAN and the sinks of NO_x from oxidation to HNO_3 and PAN. The data below 4 km are not inconsistent with a scenario where PAN produced in biomass burning plumes decomposes to sustain NO_x levels in the lower troposphere on the regional scale, but the paucity of points precludes any reliable analysis.

Above 8 km we find a systematic imbalance in the chemical

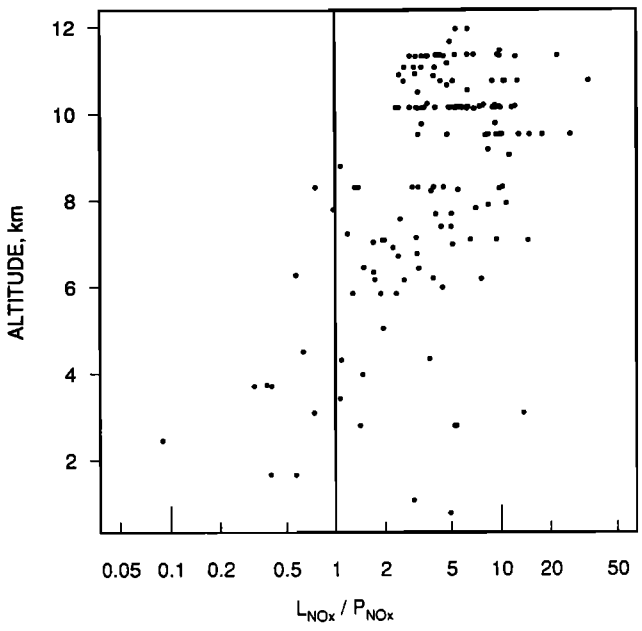

Figure 7. Ratio of 24-hour average chemical loss to chemical production rates of NO_x as a function of altitude for individual measurement time intervals in the southern hemisphere TRACE A data.

budget for NO_x (Figure 7), with production of NO_x balancing on average only 16% of the loss. This deficit is due to insufficient recycling of HNO_3 to NO_x; recycling of PAN is not an issue because rates for NO_x-PAN cycling are slow and PAN is near chemical steady state (Table 5). The median rate of conversion of NO_x to HNO_3 at 8-12 km in the model is 57 pptv day^{-1}, while the median observed HNO_3 concentration at that altitude is 59 pptv. A HNO_3 lifetime of 1 day would be necessary to balance the HNO_3 budget, but the median lifetime of HNO_3 against photolysis and reaction with OH is 12 days. It thus appears that a major mechanism for high-altitude conversion of HNO_3 to NO_x may be missing from the model. The problem would remain even if N_2O_5 conversion to HNO_3 in aerosols did not proceed, as this reaction accounts, on average, for only 30% of the conversion of NO_x to HNO_3 (Table 5).

The above analysis suggests that HNO_3 in the upper troposphere must be consumed on a timescale of 1 day to eventually regenerate NO_x. *Chatfield* (1994) proposed that rapid reaction of HNO_3 with CH_2O in acid aerosols might take place and yield NO_x and formic acid as immediate products. We find, however, no correlation between HNO_3 and NO concentrations in the TRACE A data above 8 km (Figure 8), which argues against direct conversion of HNO_3 to NO_x on a short time scale. *Fan et al.* [1994] proposed that the reaction of HNO_3 with CH_2O in acid aerosols may not produce NO_x but hydroxymethylnitrate $H_2C(OH)ONO_2$; this species could then photolyze to yield NO_x on a timescale of one week, based on laboratory data for other organic nitrates [*Barnes et al.*, 1993]. The *Fan et al.* [1994] mechanism would be more consistent with the lack of correlation between NO and HNO_3 in the TRACE A data.

7. Schematic for Ozone in the Tropical Troposphere

Our analysis of the TRACE A data suggests a simple schematic for the regional budget of tropospheric O_3 over the South Atlantic basin. Continental NO_x emissions from South America and southern Africa are pumped to the middle and upper troposphere by convection, leading to ubiquitous net production of O_3 in the upper troposphere. Eventually, the air subsides over the Atlantic Ocean and net loss of O_3 takes place. Low-level advection to the continents closes the O_3 cycle. We propose that this schematic can be extended to other tropical regions and provides a general explanation for the origin of O_3 in the tropical troposphere, as illustrated in Figure 9. In this figure, the large-scale circulation of the tropical atmosphere is represented by the

Table 5. Chemical Cycling of NO_x over the South Atlantic Basin

	Altitude Band, km		
	0-4	4-8	8-12
	Number of Model Points		
	15	37	149
NO_x loss, pptv d^{-1}			
NO_2 + OH	230	50	41
N_2O_5 + aerosol	141	37	16
CH_3CO_3 + NO_2	132	19	7
RO_2 + NO_x [a]	74	4	1
Total Loss	787	112	67
NO_x production, pptv d^{-1}			
HNO_3 photolysis	14	3	2
HNO_3 + OH	24	3	2
PAN thermolysis	728	6	<1
PAN photolysis	6	8	7
Total Production	900	31	12
NO_x lifetime, days	0.18	0.66	2.4

Median 24-hour average rates and lifetimes computed in the model for the southern hemisphere TRACE A data. Because the values shown are medians, the sum of the individual rates does not add up to the total production or loss of NO_x, and the median lifetime does not match exactly the corresponding concentration and loss rate; this effect is particularly noticeable at 0-4 km where the scatter of rates for individual points is large and the number of points is small. The rates of production and loss of PAN have been corrected for internal cycling within the (CH_3CO_3 + PAN) family as described in Appendix B.

[a] Formation of all organic nitrates other than PAN. These organic nitrates are assumed inert in the model.

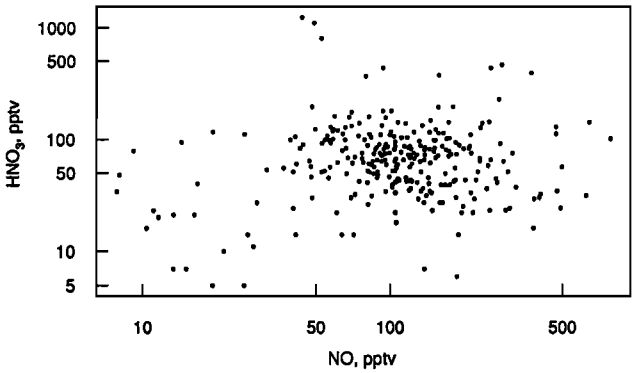

Figure 8. Relationship of HNO_3 and NO concentrations in the TRACE A daytime data (0800-1600 local time) at 8 to 12-km altitude.

Walker cells [after *Newell*, 1979]. Transfer of air from the lower to the upper troposphere takes place mainly by deep wet convection over South America, Africa, and Oceania (rising branches of the Walker cells). These convective motions inject to the upper troposphere NO_x emitted over the continents by combustion and soils, and additional NO_x produced by lightning in the convective column. The injection of NO_x then drives O_3 production in the upper troposphere. It must be pointed out that although production of O_3 in the upper troposphere is necessary to explain the observed increase of O_3 concentrations with altitude and to balance the net O_3 loss in the lower troposphere, most of the O_3 production in the tropospheric column actually takes place in the lower and middle troposphere (Figure 4).

Some support for the schematic in Figure 9 is offered by data from the equatorial Pacific. *Piotrowicz et al.* [1991] found that the distribution of O_3 concentrations in surface air over the equatorial Pacific is highly sensitive to seasonal and interannual movements of the Pacific Walker cell. *Fishman et al.* [1990] reported a west-to-east gradient of increasing tropospheric O_3 columns across the Pacific which may be explained by net O_3 production in the upper troposphere westerlies and net loss in the lower troposphere easterlies. It is well established that the lower troposphere of the equatorial Pacific is a net sink for O_3 [*Liu et al.*, 1983; *Johnson et al.*, 1990]. Limited aircraft data for the western tropical Pacific indicate net O_3 loss taking place below 6-km altitude and net production taking place above, with O_3 production balancing 60% of O_3 loss in the 0 to 12-km column [*Davis et al.*, 1996].

Our representation of the budget of O_3 in the tropical troposphere goes back to the earliest papers arguing that the tropospheric O_3 budget is dominated by in situ production and that transport from the stratosphere is small in comparison [*Chameides and Walker*, 1973; *Crutzen*, 1973; *Fishman et al.*, 1979; *Liu et al.*, 1980]. Much uncertainty was attached to these early studies because of the lack of reliable NO data. *Liu et al.* [1980] first proposed the idea of a photochemical steady state of O_3 in the tropospheric column with net production in the upper troposphere compensating for net loss in the lower troposphere. They argued that the NO_x in the upper troposphere driving the in situ production would originate from the stratosphere, but the TRACE A data as well as previous work [*Kasibhatla et al.*, 1991; *Penner et al.*, 1991; *Murphy et al.*, 1993] show that stratospheric influx is negligible compared to combustion and lightning as a source of NO_x in the tropical upper troposphere.

8. Conclusions

Photochemical modeling of TRACE A aircraft observations over the South Atlantic basin up to 12-km altitude indicates a close balance between chemical production and loss of O_3 in the 0 to 12-km column, with net production in the upper troposphere balancing weak net loss in the lower troposphere. Influx from the stratosphere is unimportant as a source of tropospheric O_3 in the region. We conclude that the tropospheric O_3 column can be maintained solely by in situ photochemistry. The photochemical production of O_3 is limited by the supply of NO_x, even in the upper troposphere. Past observations of the remote troposphere indicate that NO_x concentrations are generally near the turnover point for net O_3 production versus net O_3 loss; we interpret this observation as reflecting the tendency of O_3 concentrations to adjust to a chemical steady state defined by the available NO_x.

Biomass burning and lightning were the two primary sources of NO_x over the South Atlantic basin in TRACE A. Considering the short lifetime of NO_x against oxidation (only 2-3 days at 8-12 km altitude), it appears that the high NO_x levels observed throughout the South Atlantic basin were maintained by chemical recycling of NO_x from its oxidation products. The low HNO_3/NO concentration ratios observed above 8 km imply rapid conversion of HNO_3 to NO_x by a mechanism not considered in current models.

We presented a simple schematic for the origin of O_3 in the South Atlantic basin troposphere linking the large-scale Walker circulation to in situ photochemistry. Convection over South America and southern Africa injects NO_x from combustion, soils, and lightning to the middle and upper troposphere, leading to net

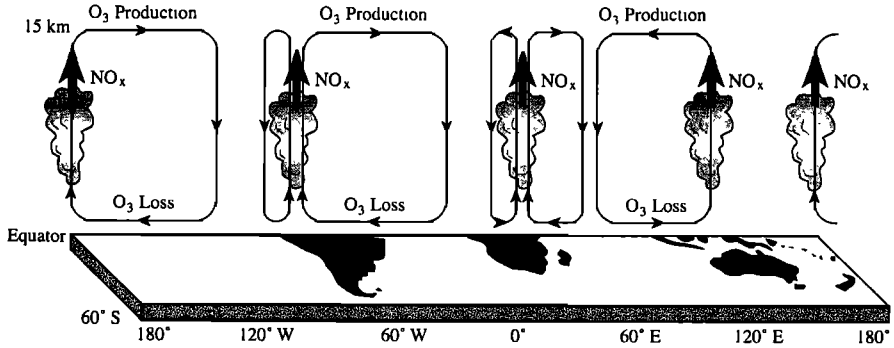

Figure 9. Schematic depiction of the O_3 budget in the tropical troposphere. Net O_3 production in the upper troposphere balances net O_3 loss in the lower troposphere. Mass exchange between the lower and the upper troposphere is represented by the Walker circulation [after *Newell*, 1979]. Deep convective motions over South America, southern Africa, and Oceania (rising branches of the Walker circulation) inject NO_x from combustion, soils, and lightning to the upper troposphere, driving O_3 production. Eventually, the air subsides over the oceans and net O_3 loss takes place in the lower troposphere due to low NO_x concentrations and high humidities, closing the O_3 cycle.

O_3 production; eventually, the air subsides over the Atlantic Ocean and net loss of O_3 takes place in the lower troposphere due to reduced NO_x levels and high humidities. Low-level advection of marine air to the continents closes the O_3 cycle. We proposed that the same schematic applies to other tropical regions and offers a general representation of the O_3 budget in the tropical troposphere. This mechanism would imply a great sensitivity of the global oxidizing power of the atmosphere to NO_x emissions from tropical continents.

Peroxide concentrations measured aboard the aircraft in TRACE A offered a sensitive test of the O_3 production and loss rates computed in our photochemical model. We found that the model captures 78% and 74% of the observed variances of H_2O_2 and CH_3OOH concentrations, respectively. Below 8-km altitude there is no mean bias for H_2O_2 and a 30% negative bias for CH_3OOH. Above 8-km the model underestimates H_2O_2 by a factor of 1.8 and CH_3OOH by a factor of 3.6. Even allowing for these discrepancies, the agreement between modeled and observed peroxide concentrations is sufficiently good to lend confidence in our conclusions regarding the O_3 budget in the tropospheric column.

Formaldehyde concentrations measured aboard the aircraft provided another test of photochemistry in the model. The model captures 62% of the variance of measured CH_2O concentrations but tends to overestimate concentrations in the lower troposphere (0-4 km) and underestimate concentrations in the middle troposphere (4-8 km). The largest discrepancy between model and observations is in the marine boundary layer, where the model is too high by a factor of 3. A review of previous data in the tropical marine boundary layer indicates considerable variability in measured CH_2O concentrations that cannot be explained with current models. The issue requires further investigation.

Appendix A: Photochemical Model

Our photochemical mechanism includes inorganic and methane chemistry from *DeMore et al.* [1994], and non-methane hydrocarbon chemistry from *Atkinson et al.* [1993] and *Atkinson* [1994]. The rate constant and branching ratio for the $CH_3OOH+OH$ reaction are from *Vaghjiani and Ravishankara* [1989]. The yield of $O(^1D)$ from photolysis of O_3 is from *Michelsen et al.* [1994]. Recent data are used for the photolysis of HNO_3 [*Burkholder et al.*, 1993], PAN [*Talukdar et al.*, 1995], and ketones [*Raber and Moortgaat*, 1995].

Hydrolysis of N_2O_5 to HNO_3 in aerosols is included with a rate constant determined by the collision frequency of N_2O_5 molecules on aerosol particles [*Fuchs and Sutugin*, 1971] and a reaction probability of 0.1 based on data for aqueous surfaces [*DeMore et al.*, 1994]. The collision frequency is computed using the aerosol size distribution (range 0.12 to 2 μm radius) measured aboard the aircraft with 10-s resolution. The reaction probability of N_2O_5 on the aerosol surface would be low if the aerosol were solid [*Mozurkewich and Calvert*, 1988]. At the temperatures and humidities found above 8-km altitude in TRACE A, the stable phase of the binary H_2SO_4-H_2O system is usually solid $H_2SO_4 \bullet 4H_2O$ (sulfuric acid tetrahydrate, or SAT). The reaction probability of N_2O_5 on SAT is only 0.001-0.01 [*Hanson and Ravishankara*, 1993]. However, the aerosol could be in a metastable liquid state. Considering that our model uses NO as an input variable, the inclusion of N_2O_5 hydrolysis has no significant effect on the model photochemistry, but it provides a significant term in the computed mass balance for NO_x. On the one hand, the rate of hydrolysis could be underestimated if there is significant aerosol surface area outside of the 0.12 to 2-μm particle size range; on the other hand, it could be overestimated if the aerosol includes a significant population of dry particles.

Photolysis frequencies are computed at each point using the clear-sky radiation model of *Logan et al.* [1981] with a surface albedo of 0.1. They are then scaled for cloud and albedo effects using a factor $CF = J_{NO_2,Eppley}/J_{NO_2,clear}$, where $J_{NO_2,clear}$ is the clear-sky NO_2 photolysis frequency computed with the radiation model at the local time of observation, and $J_{NO_2,Eppley}$ is the value derived from the Eppley UV radiometer measurements using the parameterization of *Madronich* [1987], as described by *Davis et al.* [1993]. This parameterization is applicable only to solar zenith angles less than 70° and we therefore restrict our calculations to this range (97% of observations). Mean CF values in TRACE A were 0.99 at 0-2 km and 1.35 at 8-12 km; values of CF higher than 2 (maximum 2.51) were found when the aircraft flew through clouds or above stratus decks under high-Sun conditions. There was no significant dependence of CF on Sun angle. To check for consistency between the J_{NO_2} values computed from our clear-sky radiation model and those inferred from the Eppley data, we searched for cloud-free conditions in the aerosol lidar data and in videos taken from forward and nadir cameras aboard the aircraft. The only unambiguous clear-sky period was on flight 12 over Namibia (1200-1240 GMT), with the aircraft cruising at 10-km altitude. The mean CF for this period was 1.06.

Model results for CH_3OOH and CH_2O are sensitive to the oxidation mechanism assumed for acetic acid. Acetic acid concentrations measured in TRACE A averaged 2-3 ppbv throughout the 0 to 12-km column (Table 1a). No laboratory data are available to our knowledge for the products of acetic acid oxidation by OH. The mechanism proposed by *Atkinson* [1994],

$$CH_3COOH + OH \xrightarrow{O_2} CH_3O_2 + CO_2 + H_2O \qquad (A1)$$

would result in acetic acid providing a major source of CH_3OOH and CH_2O in the upper troposphere; at 230 K, 3 ppbv of acetic acid would produce as much CH_2O as 1700 ppbv of CH_4. However, the TRACE A data show no correlation between measured acetic acid and CH_2O in the upper troposphere, even when measured acetic acid is as high as 8 ppbv (Figure A1). We conclude that either there is an error in the measurements, or the oxidation of acetic acid does not produce CH_2O. To side step this problem, we assume for the purposes of the model that the oxidation of acetic acid follows the scheme of *Madronich and Calvert* [1989], which bypasses CH_3OOH and CH_2O formation:

$$CH_3COOH + OH \xrightarrow{O_2} CH_2(O_2)COOH + H_2O \qquad (A2)$$

$$CH_2(O_2)COOH + NO \rightarrow CH_2(O)COOH + NO_2 \qquad (A3)$$

$$CH_2(O)COOH + O_2 \rightarrow CHOCOOH + HO_2 \qquad (A4)$$

$$CHOCOOH + OH \xrightarrow{O_2} + CO + CO_2 + H_2O + HO_2 \qquad (A5)$$

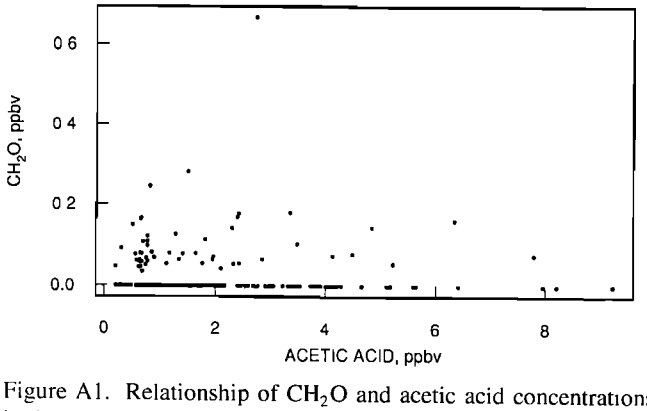

Figure A1. Relationship of CH_2O and acetic acid concentrations in the TRACE A data at 8 to 12-km altitude.

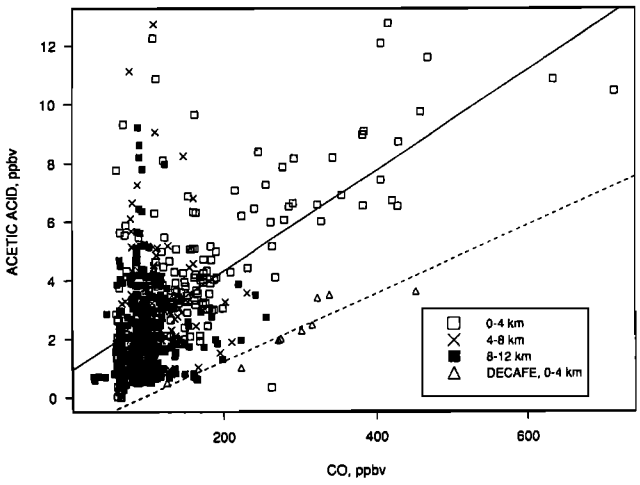

Figure A2. Relationship of acetic acid and CO concentrations in the southern hemisphere TRACE A data (squares, crosses) and in the DECAFE aircraft data over the Congo rainforest [*Helas et al.*, 1992]. The solid and dashed lines are linear best fits to the TRACE A and DECAFE data, respectively. The DECAFE data set consists of only 10 points.

When NO concentrations are low, formation of the organic peroxide $CH_2(OOH)COOH$ provides a temporary reservoir but does not change the ultimate fate of the carbon. With this mechanism, acetic acid has little effect on the model photochemistry even at the high concentrations measured in TRACE A.

The origin of the high acetic acid concentrations observed in TRACE A remains a puzzle. There are to our knowledge no previous observations in the upper troposphere that can be used for comparison. Figure A2 shows the relationship between acetic acid and CO in TRACE A, and compares to the relationship found in 10 dry season measurements taken at 0-4 km over the Congo rainforest during the Dynamique et Chimie en Forêt Equatoriale (DECAFE) expedition [*Helas et al.*, 1992]. Both the TRACE A and the DECAFE data show correlations between acetic acid and CO at 0-4 km, with similar slopes, indicating acetic acid emission from biomass burning; however, the TRACE A data include, also, a major component not correlated with CO, resulting in acetic acid concentrations about 3 ppbv higher than in DECAFE for the same amount of CO. The acetic acid concentrations measured in the upper troposphere in TRACE A were not correlated with CO or any of the other variables measured aboard the aircraft except formic acid. They do, however, show a pattern of higher values over Brazil and Africa than over the South Atlantic.

Appendix B: Treatment of NO_x-PAN Interconversion in NO_x Budget Calculations

When assessing the importance of NO_x-PAN interconversion in a regional NO_x budget calculation constrained with observations for NO_x (or NO) and PAN, and with CH_3CO_3 taken to be at steady state, one must correct the rates of reactions (10), (13), and (14) to account for cycling within the chemical family PAN_x = CH_3CO_3 + PAN. To illustrate the need for this correction, consider a situation where reactions (10), (13), and (14) dominate the production and loss of CH_3CO_3. Under this situation, given any specified input pair of NO_x and PAN concentrations, the steady state CH_3CO_3 concentration computed in the model yields an apparent steady state between NO_x and PAN; this steady state plays, however, no role in regulating NO_x since loss of NO_x and CH_3CO_3 by reaction (10) forces production of NO_x by reactions (13) and (14) to maintain the CH_3CO_3 steady state. Use of uncorrected rates R_{10}, R_{13}, and R_{14} to construct a NO_x budget can lead to the illusion of a close balance between production and loss of NO_x and to an underestimate of the chemical lifetime of NO_x.

We account for this effect in our NO_x budget analyses by using corrected rates R':

$$R'_{10} = R_{10}\frac{P_{PANx}}{P_{PANx} + R_{13} + R_{14}} \quad \text{(B1)}$$

$$R'_{13} = R_{13}\frac{L_{PANx}}{P_{PANx} + R_{13} + R_{14}} \quad \text{(B2)}$$

$$R'_{14} = R_{14}\frac{L_{PANx}}{P_{PANx} + R_{13} + R_{14}} \quad \text{(B3)}$$

where P_{PANx} and L_{PANx} are the chemical production and loss rates of the PAN_x family. In the TRACE A data set, the correction factor $P_{PANx}/(P_{PANx} + R_{13} + R_{14})$ ranges from 0.03 to 0.72 at 0-4 km and from 0.80 to 0.99 at 8-12 km. The correction factor $L_{PANx}/(P_{PANx} + R_{13} + R_{14})$ ranges from 0.23 to 0.71 at 0-4 km and from 0.76 to 0.97 at 8-12 km. The largest corrections are in the lower troposphere, where thermal decomposition of PAN often dominates the CH_3CO_3 source.

Acknowledgements. This work was supported by the NASA Global Tropospheric Chemistry Program and by the National Science Foundation (ATM-93-20778). We thank G.M. Gardner for compiling the merged time series, A.M. Thompson for providing us with the TOMS O_3 data, V.W.J.H. Kirchhoff and two reviewers for insightful comments, and J.H. Yin for producing the color Figures.

References

Anderson, B E, G.L. Gregory, J.D W. Barrick, J.E. Collins, G.W Sachse, C.H. Hudgins, J.D. Bradshaw, and S.T. Sandholm, Factors influencing dry season ozone distributions over the tropical south Atlantic, *J. Geophys. Res., 98,* 23,491-23,500, 1993.

Andreae, M.O., B.E. Anderson, D.R. Blake, J.D. Bradshaw, J.E. Collins, G.L. Gregory, G.W. Sachse, and M.C. Shipham, Influence of plumes from biomass burning on atmospheric chemistry over the equatorial and tropical South Atlantic during CITE 3, *J. Geophys. Res., 99,* 12,793-12,808, 1994.

Arlander, D.W., D.R. Cronn, J.C. Farmer, F.A. Menzia, and H.H. Westberg, Gaseous oxygenated hydrocarbons in the remote marine troposphere, *J. Geophys. Res., 95,* 16,391-16,403, 1990.

Atkinson, R.A., Gas-phase tropospheric chemistry of organic compounds, *J. Phys. Chem. Ref. Data, 2,* 1-261, 1994.

Atkinson, R., D.L. Baulch, R.A. Cox, R.F. Hampson Jr., J.A. Kerr, and J. Troe, Evaluated kinetic and photochemical data for atmospheric chemistry, supplement I, V, IUPAC subcommittee on gas kinetic data evaluation for atmospheric chemistry, *J. Phys. Chem Ref. Data, 21,* 1125-1568, 1993.

Barnes, I., K.H. Becker, and T. Zhu, Near UV absorption spectra and photolysis products of difunctional organic nitrates: Possible importance as NO_x reservoirs, *J. Atmos. Chem., 17,* 353-373, 1993.

Brasseur, G.P., D.A. Hauglustaine, and S. Walters, Chemical compounds in the remote Pacific troposphere: Comparison between MLOPEX measurements and chemical-transport-model calculations, *J. Geophys. Res., 101,* 14,795-14,813, 1996.

Brauers, T., and A. Hofzumahaus, Latitudinal variation of measured NO_2 photolysis frequencies over the Atlantic Ocean between 50°N and 30°S, *J. Atmos. Chem., 15,* 269-282, 1992.

Browell, E.V., G.L. Gregory, R.C. Harriss, and V.W.J.H. Kirchhoff, Ozone and aerosol distributions over the Amazon Basin during the wet season, *J. Geophys. Res., 95,* 16,887-16,902, 1990.

Browell, E.V., et al., Ozone and aerosol distributions and air mass characteristics over the South Atlantic basin, Africa during the burning season, *J. Geophys. Res.*, this issue.

Burkholder, J.B., R.K. Talukdar, A.R. Ravishankara, and S. Solomon, Temperature dependence of the HNO_3 UV absorption cross sections, *J. Geophys. Res., 98,* 22,937-22,948, 1993.

Carlier, P., P. Fresnet, V. Lescoat, S. Pashalidis, and G. Mouvier, Formaldehyde background levels over the Atlantic Ocean during the POLARSTERN crossing from Bremerhaven to Rio Grande Do Sul, in *Physico-Chemical Behavior of Atmospheric Pollutants*, pp. 669-674, Kluwer Acad., Norwell, Mass., 1991.

Carroll, M.A., and A.M. Thompson, NO_x in the non-urban troposphere, in *Progress and Problems in Atmospheric Chemistry*, edited by J. Barker, World Sci., River Edge, N.J., 1995.

Carroll, M.A., B.A. Ridley, D.D. Montzka, G. Hubler, J.G. Walega, R.B. Norton, B.J. Huebert, and F.E. Grahek, Measurements of nitric oxide and nitrogen dioxide during the Mauna Loa Photochemistry Experiment, *J. Geophys. Res., 97*, 10,361-10,374, 1992.

Chameides, W.L., and J.C.G. Walker, A photochemical theory of tropospheric ozone, *J. Geophys. Res., 78*, 8751-8760, 1973.

Chameides, W. L., D. D. Davis, M. O. Rodgers, J. Bradshaw, S. Sandholm, G. Sachse, G. Hill, G. Gregory, and R. Rasmussen, Net ozone photochemical production over the eastern and central North Pacific as inferred from GTE/CITE 1 observations during fall 1983, *J. Geophys. Res., 92*, 2131-2152, 1987.

Chameides, W.L., et al., Observed and model-calculated NO_2/NO ratios during the NASA GTE/CITE 2 field study, *J. Geophys. Res., 95*, 10,235-10,247, 1990.

Chatfield, R.B., Anomalous HNO_3/NO_x ratio of remote tropospheric air. Conversion of nitric acid to formic acid and NO_x?, *Geophys. Res. Lett., 21*, 2705-2708, 1994.

Crawford, J., et al., A photostationary state analysis of the NO_2-NO system based on airborne observations from the western and central North Pacific, *J. Geophys Res., 101*, 2053-2072, 1996

Crutzen, P., A discussion of the chemistry of some minor constituents in the stratosphere and troposphere, *Pure Appl. Geophys., 106-108*, 1385-1399, 1973.

Davis, D.D., et al., A photostationary state analysis of the NO_2-NO system based on airborne observations from the subtropical/tropical North and South Atlantic, *J. Geophys. Res., 98*, 23,501-23,523, 1993.

Davis, D.D., et al., Assessment of ozone photochemistry in the North Pacific as inferred from PEM-West A observations during fall 1991, *J Geophys Res., 101*, 2111-2134, 1996.

DeMore, W.B., S.P. Sander, D.M. Golden, R.F. Hampson, M.J Kurylo, C.J. Howard, A.R. Ravishankara, C.E. Kolb, and M.J Molina, Chemical kinetics and photochemical data for use in stratospheric modeling, *JPL Publ. 94-26*, Pasadena, Calif, 1994.

Dibb, J.E., R.W. Talbot, K.I. Klemm, G.L. Gregory, H B. Singh, J D Bradshaw, and S.T. Sandholm, Asian influence over the western North Pacific during the fall season: inferences from lead 210, soluble ionic species, and ozone, *J. Geophys. Res., 101*, 1779-1792, 1996

Drummond, J.W, D.H. Ehhalt, and A. Volz, Measurements of nitric oxide between 0 and 12 km altitude and 67°N to 60°S latitude obtained during STRATOZ III, *J. Geophys. Res., 93*, 15,831-15,849, 1988.

Fan, S -M., S.C. Wofsy, P.S. Bakwin, D.J. Jacob, and D R. Fitzjarrald, Atmosphere-biosphere exchange of CO_2 and O_3 in the central Amazon forest, *J. Geophys. Res., 95*, 16,851-16,864, 1990.

Fan, S.-M., D.J. Jacob, D.L. Mauzerall, J.D Bradshaw, S.T. Sandholm, D.R. Blake, R.W. Talbot, G.L. Gregory, and G.W. Sachse, Origin of tropospheric NO_x over subarctic eastern Canada in summer, *J. Geophys. Res., 99*, 16,867-16,877, 1994.

Fishman, J., S. Solomon, and P.J. Crutzen, Observational and theoretical evidence in support of a significant in-situ photochemical source of tropospheric ozone, *Tellus, 31*, 432-446, 1979.

Fishman, J., C.E. Watson, J.C. Larsen, and J.A. Logan, Distribution of tropospheric ozone determined from satellite data, *J. Geophys. Res., 95*, 3599-3618, 1990.

Fishman, J., J.M. Hoell Jr., R.D. Bendura, V.W.J.H. Kirchhoff, and R.J. McNeal Jr., The NASA GTE TRACE A Experiment (September-October 1992): Overview, *J. Geophys. Res.*, this issue.

Fuchs, N.A., and A.G. Sutugin, High-dispersed aerosols, in *International Reviews of Aerosol Physics and Chemistry, 2* edited by G.M Hidy and J.R. Brock, pp.1-60, Pergamon, New York, 1971.

Gidel, L.T., and M.A. Shapiro, General circulation estimates of the net vertical flux of ozone in the lower stratosphere and the implications for the tropospheric ozone budget, *J. Geophys. Res., 85*, 4049-4058, 1980.

Graustein, W.C., and K.K. Turekian, ^{7}Be and ^{210}Pb trace sources of ozone in the summertime subtropical free troposphere of the eastern North Atlantic, *Geophys. Res. Lett., 23*, 539-542, 1996.

Gregory, G.L., H.E. Fuelberg, S.P. Longmore, B.E. Anderson, J.E. Collins, and D.R. Blake, Chemical characteristics of tropospheric air over the tropical South Atlantic Ocean: Relationship to trajectory history, *J. Geophys. Res.*, this issue.

Hanson, D.R., and A.R. Ravishankara, Reaction of $ClONO_2$ with HCl on NAT, NAD, and frozen sulfuric acid and hydrolysis of N_2O_5 and $ClONO_2$ on frozen sulfuric acid, *J. Geophys. Res., 98*, 22,931-22,936, 1993.

Harris, G.W., D. Klemp, T. Zenker, and J.P. Burrows, Tunable diode laser measurements of trace gases during the 1988 *Polarstern* cruise and intercomparisons with other methods, *J. Atmos. Chem., 15*, 315-326, 1992.

Heikes, B.G., Formaldehyde and hydroperoxides at Mauna Loa Observatory, *J. Geophys. Res., 97*, 18,001-18,013, 1992.

Heikes, B.G., M. Lee, D. Jacob, R. Talbot, and J. Bradshaw, Ozone hydroperoxides, oxides of nitrogen, and hydrocarbon budgets in the marine boundary layer over the South Atlantic, *J. Geophys. Res.*, this issue.

Helas, G., H. Bingemer, and M.O. Andreae, Organic acids over equatorial Africa: Results from DECAFE 88, *J. Geophys. Res., 97*, 6187-6193, 1992.

Hirsch, R M., and E.J. Gilroy, Methods of fitting a straight line to data. Examples in water resources, *Water Res. Bull., 20*, 705-711, 1984.

Hofzumahaus, A., T. Brauers, U. Platt, and J. Callies, Latitudinal variation of measured O_3 photolysis frequencies $J(O^1D)$ and primary OH production rates over the Atlantic Ocean between 50°N and 30°S, *J. Atmos. Chem., 15*, 283-298, 1992.

Holton, J.R., On the global exchange of mass between the stratosphere and troposphere, *J. Atmos. Sci., 47*, 392-395, 1990.

Jacob, D. J., and S. C. Wofsy, Photochemistry of biogenic emissions over the Amazon forest, *J. Geophys. Res., 93*, 1477-1486, 1988.

Jacob, D.J , and S.C. Wofsy, Budgets of reactive nitrogen, hydrocarbons, and ozone over the Amazon forest during the wet season, *J. Geophys Res., 95*, 16,737-16,754, 1990.

Jacob, D J., et al., Summertime photochemistry at high northern latitudes, *J. Geophys. Res , 97*, 16,421-16,431, 1992

Jacob, P , and D. Klockow, Hydrogen peroxide measurements in the marine atmosphere, *J. Atmos. Chem., 15*, 353-360, 1992

Johnson, J.E., R.H. Gammon, J. Larsen, T.S. Bates, S J. Oltmans, and J C. Farmer, Ozone in the marine boundary layer over the Pacific and Indian Oceans: Latitudinal gradients and diurnal cycles, *J. Geophys. Res., 95*, 11,847-11,856, 1990.

Kasibhatla, P.S., H. Levy, W.J. Moxim, and W.L. Chameides, The relative importance of stratospheric photochemical production on tropospheric NO_y levels: A model study, *J. Geophys. Res., 96*, 18,631-18,646, 1991.

Kasibhatla, P S., H. Levy II, and W.J. Moxim, Global NO_x, HNO_3, PAN, and NO_y distributions from fossil-fuel combustion emissions A model study, *J. Geophys. Res., 98*, 7165-7181, 1993.

Kirchhoff, V.W.J.H., R.A. Barnes, and A.L. Torres, Ozone climatology at Natal Brazil, from in situ ozonesonde data, *J. Geophys. Res., 96*, 10,899-10,909, 1991.

Kirchhoff, V.W.J.H., J. R. Alves, F. R. da Silva, and J. Fishman, Observations of ozone concentrations in the Brazilian cerrado during the TRACE A field expedition, *J. Geophys. Res.*, this issue.

Klippel, W., and P. Warneck, The formaldehyde content of the atmospheric aerosol, *Atmos. Environ., 14*, 809-818, 1980.

Krishnamurti, T.N., H.E. Fuelberg, M.C. Sinha, D. Oosterhof, E L. Bensman, and V.B. Kumar, The meteorological environment of the tropospheric ozone maximum over the tropical South Atlantic, *J. Geophys. Res., 98*, 10,621-10,641, 1993.

Levy, H., II, and W. J. Moxim, Simulated global distribution and deposition of reactive nitrogen emitted by fossil fuel combustion, *Tellus, 41B*, 256-271, 1989.

Levy, H. II, J.D Mahlman, W.J. Moxim, and S.C. Liu, Tropospheric ozone: The role of transport, *J. Geophys. Res., 90*, 3753-3772, 1985.

Liu, S.C., D. Kley, M. McFarland, J.D. Mahlman, and H. Levy II, On the origin of tropospheric ozone, *J. Geophys Res., 85*, 7546-7552, 1980.

Liu, S.C., M. McFarland, D. Kley, O. Zafiriou, and B. Huebert, Tropospheric NO_x and O_3 budgets in the equatorial Pacific, *J. Geophys. Res., 88*, 1360-1368, 1983.

Liu, S C , et al., A study of the photochemistry and ozone budget during the Mauna Loa Observatory Photochemistry Experiment, *J. Geophys. Res., 97*, 10463-10471, 1992.

Logan, J.A., and V.W.J.H. Kirchhoff. Seasonal variations of tropospheric ozone at Natal, Brazil, *J. Geophys. Res., 91*, 7875-7881, 1986.

Logan, J.A., M.J. Prather, S.C. Wofsy, and M.B. McElroy, Tropospheric

chemistry: A global perspective, *J. Geophys. Res., 86,* 7210-7254, 1981.

Loring, R.O., Jr., H.E. Fuelberg, and J. Fishman, The role of middle latitude cyclones on the distribution of ozone over the South Atlantic Ocean, *J. Geophys. Res.*, this issue.

Lowe, D.C., and U. Schmidt, Formaldehyde (HCHO) measurements in the nonurban troposphere, *J. Geophys. Res., 88,* 10,844-10,858, 1983

Madronich, S., Intercomparison of NO_2 photodissociation and UV radiometer measurements, *Atmos. Environ., 21,* 569-578, 1987.

Madronich, S., and J.G. Calvert, The NCAR master mechanism of the gas phase chemistry - Version 2.0, *NCAR Tech. Note, NCAR/TN-333+STR,* Natl. Cent. for Atmos. Res., Boulder, Colo , 1989.

Mauzerall, D.L., D J. Jacob, S.-M. Fan, J.D. Bradshaw, G.L. Gregory, G.W. Sachse, and D.R. Blake, Origin of tropospheric ozone at remote high northern latitudes in summer, *J. Geophys. Res., 101,* 4175-4188, 1996.

Michelsen, H.A., R.J. Salawitch, P.O. Wennberg, and J.G. Anderson, Production of $O(^1D)$ from photolysis of O_3, *Geophys. Res. Lett., 21,* 2227-2230, 1994.

Mozurkewich, M., and J. G. Calvert, Reaction probability of N_2O_5 on aqueous aerosols, *J. Geophys. Res., 93,* 15,889-15,896, 1988.

Murphy, D., D. Fahey, M. Proffitt, S. Liu, C. Eubank, S. Kawa, and K. Kelly, Reactive odd nitrogen and its correlation with ozone in the lower stratosphere and upper troposphere, *J. Geophys. Res., 98,* 8751-8773, 1993.

Newell, R.E., Climate and the ocean, *Am. Sci , 67,* 405-416, 1979

Olson, J., J. Fishman, and V.W.J.H. Kirchhoff, Analysis of the distribution of ozone over the southern Atlantic region, *J. Geophys. Res* , this issue.

Penner, J.E., C.S. Atherton, J. Dignon, S.J. Ghan, J.J. Walton, and S Hameed, Tropospheric nitrogen: A three-dimensional study of sources, distributions, and deposition, *J Geophys. Res., 96,* 959-990, 1991.

Pickering, K.E., et al., Convective transport of biomass burning emissions over Brazil during TRACE A, *J. Geophys. Res.*, this issue.

Piotrowicz, S.R., H.F. Bezdek, G.R. Harvey, M. Springer-Young, and K.J. Hanson, On the ozone minimum over the equatorial Pacific Ocean, *J Geophys Res, 96,* 18,679-18,687, 1991.

Platt, U , J Rudolph, T. Brauers, and G W Harris, Atmospheric measurements during *Polarstern* cruise ANT VII/1, 54°N to 32°S: An overview, *J. Atmos. Chem., 15,* 203-214, 1992.

Prather, M.J., R. Derwent, D. Ehhalt, P. Fraser, E. Sanhuenza, and X. Zhou, Other trace gases and atmospheric chemistry, in *Climate Change 1994,* edited by J.T. Houghton et al., pp. 73-126, Cambridge University Press, Cambridge, New York, 1995.

Raber, W H , and G.K. Moortgaat, Photooxidation of selected carbonyl compounds in air: Methyl ethyl ketone, methyl vinyl ketone, methacrolein and methyl glyoxal, in *Progress and Problems in Atmospheric Chemistry,* edited by J. Barker, World Sci., River Edge, N.J., 1995.

Singh, H.B., D. Herlth, D. O'Hara, L. Salas, A.L Torres, G.L. Gregory, G.W. Sachse, and J.F. Kasting, Atmospheric peroxyacetyl nitrate measurements over the Brazilian Amazon Basin during the wet season: Relationships with nitrogen oxides and ozone, *J. Geophys. Res., 95,* 16,945-16,954, 1990.

Singh, H.B., M. Kanakidou, P.J. Crutzen, and D J Jacob, High concentrations and photochemical fate of oxygenated hydrocarbons in the global troposphere, *Nature, 378,* 50-54, 1995.

Singh, H.B., et al., Impact of biomass burning emissions on the composition of the South Atlantic troposphere: Reactive nitrogen and ozone, *J Geophys. Res.*, this issue.

Smyth, S , et al , Factors influencing the upper free tropospheric distribution of reactive nitrogen over the South Atlantic during the TRACE A experiment, *J. Geophys. Res.*, this issue.

Talbot, R.W., et al., Chemical characteristics of continental outflow over the tropical South Atlantic Ocean from Brazil and Africa, *J. Geophys. Res.*, this issue.

Talukdar, R.K., J.B. Burkholder, A.-M. Scholtner, J.M. Roberts, and A.R. Ravishankara, Investigation of the loss processes for peroxyacetyl nitrate in the atmosphere: UV photolysis and reaction with OH, *J. Geophys. Res., 100,* 14,163-14,173, 1995.

Thompson, A.M., The oxidizing capacity of the earth's atmosphere: Probable past and future changes, *Science, 256,* 1157-1165, 1992.

Thompson, A M., and R.W. Stewart, Effect of chemical kinetics uncertainties on calculated constituents in a tropospheric chemical model, *J Geophys. Res., 96,* 13,089-13,108, 1991.

Thompson, A.M., and O.C. Zafiriou, Air-sea fluxes of transient atmospheric species, *J. Geophys. Res., 88,* 6696-6708, 1983.

Thompson, A.M., et al., Where did tropospheric ozone over southern Africa and the tropical Atlantic come from in October 1992? Insights from TOMS, GTE TRACE A, and SAFARI-1992, *J. Geophys. Res.*, this issue.

Vaghjiani, G.L., and A.R. Ravishankara, Kinetics and mechanism of OH reaction with CH_3OOH, *J. Phys. Chem., 93,* 1948-1959, 1989.

Wofsy, S.C., et al., Atmospheric chemistry in the Arctic and Subarctic: Influence of natural fires, industrial emissions, and stratospheric inputs, *J. Geophys. Res., 97,* 16,731-16,746, 1992.

Zafiriou, O C., J. Alford, M. Herrera, T. Peltzer, and S.C. Liu, Formaldehyde in remote marine air and rain: Flux measurements and estimates, *Geophys. Res. Lett., 7,* 341-344, 1980.

Zhou, X , Y.-N. Lee, L. Newman, X. Chen, and K. Mopper, Tropospheric formaldehyde concentration at Mauna Loa Observatory during MLOPEX II, *J. Geophys. Res., 101,* 14,711-14,719, 1996.

D. R. Blake, Department of Chemistry, University of California at Irvine, Irvine, CA 92717.

J D Bradshaw, School of Earth and Atmospheric Sciences, Georgia Institute of Technology, Atlanta, GA 30332-0340.

S. M. Fan, Department of Geology and Geophysical Sciences, Princeton University, Princeton, NJ 08542.

G L. Gregory and G. W. Sachse, NASA Langley Research Center, MS 401 A, Hampton, VA 23665-5225.

G G. Heikes, Graduate School of Oceanography, University of Rhode Island, Narragansett, RI 02882.

D. J. Jacob (corresponding author), J. A. Logan, and D. A. Mauzerall, Department of Earth and Planetary Sciences and Division of Applied Sciences, Pierce Hall, 29 Oxford Street, Harvard University, Cambridge, MA 02138.

H B Singh, NASA Ames Research Center, MS 245 5, Moffett Field, CA 94035.

R W Talbot, Institute for the Study of Earth, Oceans, and Space, Science and Engineering Building, University of New Hampshire, Durham, NH 038;24

(Received February 24, 1995; revised December 22, 1995;
accepted January 4, 1996.)